Monthly Notices
of the
ROYAL ASTRONOMICAL SOCIETY

MNRAS **450,** 4109–4136 (2015) doi:10.1093/mnras/stv847

The 6-GHz methanol multibeam maser catalogue – V. Galactic longitudes 20°–60°

S. L. Breen,[1⋆] G. A. Fuller,[2,3] J. L. Caswell,[1†] J. A. Green,[1,4] A. Avison,[2,3] S. P. Ellingsen,[5] M. D. Gray,[2] M. Pestalozzi,[6] L. J. Quinn,[2,7] A. M. S. Richards,[2,3] M. A. Thompson[8] and M. A. Voronkov[1]

[1]*CSIRO Astronomy and Space Science, Australia Telescope National Facility, PO Box 76, Epping, NSW 1710, Australia*
[2]*Jodrell Bank Centre for Astrophysics, Alan Turing Building, School of Physics and Astronomy, University of Manchester, Manchester M13 9PL, UK*
[3]*UK ALMA Regional Centre Node, Manchester, M13 9PL, UK*
[4]*SKA Organization, Jodrell Bank Observatory, Lower Withington, Macclesfield, Cheshire SK11 9DL, UK*
[5]*School of Mathematics and Physics, University of Tasmania, Private Bag 37, Hobart, TAS 7001, Australia*
[6]*Istituto di Astrofisica e Planetologia Spaziali IAPS - INAF, via del Fosso del cavaliere 100, I-00133 Roma, Italy*
[7]*Bury College, Millennium Centre, Market Street, Bury BL9 0DB, UK*
[8]*Centre for Astrophysics Research, Science and Technology Research Institute, University of Hertfordshire, College Lane, Hatfield AL10 9AB, UK*

Accepted 2015 April 13. Received 2015 April 12; in original form 2015 March 24

ABSTRACT

We present the fifth portion of an unbiased survey of the Galactic plane, $|b| \leq 2^\circ$, for 6668-MHz methanol masers. This section of the survey completes the Galactic longitude range visible to the Parkes radio telescope, incorporating the longitude range 20°–60°. Within this section of the survey we find 265 methanol masers, 64 new to the survey, bringing the total number of methanol masers detected across the full longitude coverage (186°, through 0°, to 60°) to 972 sources.

Key words: masers – surveys – stars: formation – ISM: molecules.

1 INTRODUCTION

The Methanol Multibeam (MMB) survey is a sensitive search of the Galactic plane for the 6668-MHz methanol maser line (Green et al. 2009a). Such a search has several advantages over other maser lines, as the 6668-MHz methanol maser is not only bright and commonly observed, but is, importantly, associated exclusively with young high-mass star formation regions (Pestalozzi, Humphreys & Booth 2002; Minier et al. 2003; Xu et al. 2008; Breen et al. 2013). This, therefore, makes them excellent signposts of elusive young high-mass stars, and, combined with their tendency to trace systemic velocities (e.g. Szymczak, Bartkiewicz & Richards 2007; Caswell 2009; Pandian, Menten & Goldsmith 2009), also allows them to be used to investigate aspects such as Galactic structure (Green et al. 2011). Furthermore, in combination with other methanol maser transitions (in particular their 12.2-GHz counterparts) and methanol maser pumping models (e.g. Cragg, Sobolev & Godfrey 2005), these masers can be used to investigate the evolution of the associated high-mass star (e.g. Breen et al. 2010; Ellingsen et al. 2011), and how this relates to small changes in the physical conditions in the regions where they form.

There have been two significant complete surveys for 6668-MHz methanol masers within the 20°–60° Galactic longitude range previously. A subsection of this longitude range has been sensitively searched for 6668-MHz methanol masers with the Arecibo telescope (Pandian, Goldsmith & Deshpande 2007). The 5σ detection limit for this search was ∼0.43 Jy, allowing a total of 86 methanol masers to be detected within the search range of $35\overset{\circ}{.}2 \leq l \leq 53\overset{\circ}{.}7$, $|b| \leq 0\overset{\circ}{.}41$. These detections were subsequently followed up with either MERLIN (Multi-Element Radio Linked Interferometer Network) or the VLA (Very Large Array) to obtain precise positions (Pandian et al. 2011). A further portion of the Galactic plane was searched with the Torun telescope, covering the longitude range $20^\circ \leq l \leq 40^\circ$ and latitudes $|b| \leq 0\overset{\circ}{.}52$ to a 3σ sensitivity of 1.6 Jy (Szymczak et al. 2002). This search detected 100 6668-MHz methanol masers, many of which have been the subject of subsequent VLBI (very long baseline interferometry)-scale studies (e.g. Bartkiewicz, Szymczak & van Langevelde 2005; Niezurawska et al. 2005; Bartkiewicz et al. 2009) or positioned in various interferometric studies (Szymczak et al. 2012, and references therein). Other, smaller, targeted searches within our longitude range have typically been directed towards *IRAS* (*Infrared Astronomical Satellite*) sources (e.g. Walsh et al. 1998; Szymczak, Hrynek & Kus 2000), sources displaying far-infrared, radio continuum and molecular line data indicative of young high-mass stars (Beuther et al. 2002), colour-selected sources from the GLIMPSE (Galactic Legacy Infrared Mid-Plane

⋆E-mail: Shari.Breen@csiro.au
†Deceased 2015 January 14.

Survey Extraordinaire) survey (Ellingsen 2007; Cyganowski et al. 2009) and, most recently, Herschel infrared GALactic Plane Survey (Hi-GAL) sources (Olmi et al. 2014).

Distances measured through trigonometric parallax observations of methanol and water masers are now available for more than 100 sources (Reid et al. 2014, and references therein). This work has been concentrated in the Northern hemisphere, but recently one source was observed from the Southern hemisphere (Krishnan et al. in press). There are currently at least 25 methanol masers within our longitude range that have accurate distance measurements (Reid et al. 2014) and the ongoing maser parallax work is set to provide increasingly large sample sizes for meaningful studies of high-mass star formation regions and other aspects such as the structure of our Galaxy.

Here we present all 6668-MHz methanol masers detected in the 20–60° longitude range. This is the final portion of the series cataloguing methanol masers in the $|b| \leq 2°$ for the portion of the Galactic plane visible to the Parkes radio telescope, adding to the four catalogues already published (Caswell et al. 2010, 2011; Green et al. 2010, 2012a) to completely cover the Galactic longitude range 186° (through the Galactic Centre) to 60°. This final instalment of the catalogue will be closely followed by a further publication presenting the overall statistics of the entire MMB survey, and we therefore limit the discussion in this paper to the sources located within the 20°–60° longitude range.

2 MMB SURVEY PARAMETERS AND EQUIPMENT

A detailed account of the survey strategy and equipment have been given in Green et al. (2009a), which we will briefly summarize here. The initial search for 6668-MHz methanol masers was conducted with the Parkes 64-m radio telescope using a purpose-built seven-beam receiver. The Galactic plane was raster scanned in blocks of 2° in longitude by the full coverage of 4° in latitude (centred on the Galactic plane). Each resultant data cube was searched for methanol maser emission first using an automated routine and then visually inspected. Detected masers were then observed with an interferometer [either the ATCA (Australia Telescope Compact Array) or MERLIN] to determine precise positions. Sources which could be unambiguously identified as previous detections with precise positions were not routinely re-observed.

A sensitive Parkes spectrum was taken towards each detection, typically with a total integration time of 7 min (by cycling the on-source position through each of the seven beams for 1 min each in an 'MX' observation). An attempt was made to target these MX observations towards the precisely derived position but this only occurred ∼50 per cent of the time in this longitude range. In the absence of a precise position at the time the MX observations were made, we targeted the position determined from the survey cube which was usually well within 30 arcsec of the true position. This means that some of our flux density measurements could be biased towards slightly lower values (discussed further in Section 4.3). For this region of the survey, initial survey observations were made between 2006 and 2008 and MX observations chiefly between 2007 and 2009.

At 6668-MHz the FWHM (full width at half-maximum) beamwidth of the Parkes radio telescope is 3.2 arcmin. The typical rms noise in the survey cubes was 0.17 Jy corresponding to ∼100 per cent completeness at 1 Jy (Green et al. 2009a). The rms noise of the follow-up MXs was ∼0.07 Jy. The velocity coverage in this Galactic longitude range was 180 km s^{-1} (corresponding to 4 MHz) and the central frequency was adjusted to achieve full coverage of the CO emission from Dame, Hartmann & Thaddeus (2001). The spectral resolution was 0.11 km s^{-1}.

Detected methanol masers that had not previously been observed with an interferometer were subsequently observed with either the ATCA or MERLIN in many separate observation sessions between 2006 and 2014. All interferometric observations employed standard strategies, with observations of masers interspersed with observations of nearby phase calibrators, repeated over several hours to achieve adequate *uv*-coverage. Observations of bandpass and flux density calibrators were observed during each epoch. Data were reduced using standard data reduction packages (MIRIAD and AIPS) employing standard techniques for spectral line reduction.

3 SURVEY RESULTS

Within the longitude range of 20°–60° we detect a total of 265 methanol masers as presented in Table 1. The first column lists the Galactic coordinates, calculated from the more precise right ascension and declination given in columns 2 and 3, and used as source names throughout the paper. For three sources, precise positions were not available, and we therefore list their Galactic coordinates to two decimal places and show their right ascension and declination in italics, indicating that their positions have been derived from our survey observations. Following the source position are the lowest and highest velocities of emission detected at any of the observation epochs. The velocity of the peak emission feature and the peak flux density are then given for both the follow-up observations and the initial survey cube measurements. In some instances there is a temporal gap of as many as six years between the observation epochs. Finally, we give a reference to the listed position, either an observation epoch if new observations were made, or a reference to the literature. In three instances, we were unable to derive precise source positions (due to the sources fading below our detection limit at the time when follow-up observations were made) and present a single-dish position only, which we anticipate are well within 30 arcsec of the true position.

In some cases, there are no values listed in the columns giving the velocity and flux density of the peak emission. This primarily occurs in instances where we have no follow-up observation of our own, meaning that we have just a single measurement of these properties from the survey cube, and these are already given in columns 8 and 9.

Spectra for each of the detected methanol masers are given in Fig. 1 and are presented in order of increasing longitude unless there was a need to vertically align nearby sources which are confused with nearby emission. All spectra have a velocity range of 30 km s^{-1} and no sources showed emission beyond this range. The presented spectra are chiefly derived from MX observations carried out with Parkes, unless marked with either a '*' or '**' following the source name indicating a survey cube or ATCA spectrum, respectively. Spectra contaminated with features from nearby sources are clearly marked.

The percentage of new detections in this section of the Galactic plane is lower than other portions of the catalogue. Within the 20°–60° longitude range, we find ∼24 per cent of sources are new, compared with, for example, 43 per cent in the $186° \leq l \leq 330°$ range (Green et al. 2012a). The lower rate of new detections reflects the larger number of sensitive searches previously conducted within this range, which is accessible from the Northern hemisphere.

In some cases we have multiple precise positional measurements for a single source (from both our own observations and those

Table 1. Positions and parameters for the methanol masers detected in the 20°–60° longitude range. Positions derived from our own ATCA or MERLIN observations are indicated by an observation epoch in column 10, preceded by either an 'A' or 'M' indicating either the ATCA or MERLIN, respectively. References to positions taken from the literature are: W98: Walsh et al. (1998), Beu02: Beuther et al. (2002), Niez05: Niezurawska et al. (2005), Cyg09: Cyganowski et al. (2009), C09: Caswell (2009), Bart09: Bartkiewicz et al. (2009), Xu09: Xu et al. (2009a), Brunth09: Brunthaler et al. (2009), Pan11: Pandian et al. (2011), Mos07: Moscadelli et al. (2007), Mos11: Moscadelli, Sanna & Goddi (2011), Mos13: Moscadelli et al. (2013), Bart14: Bartkiewicz, Szymczak & van Langevelde (2014), Fuji14: Fujisawa et al. (2014b). The positions have been taken from the non-bracketed reference. Source names followed by a '†' indicate that their position, listed in italics, has been taken from the survey observations.

Source name	Equatorial coordinates		Velocity range		MX/ATCA data		Survey cube data		Position
(l, b)	RA (2000)	Dec. (2000)	V_L	V_H	V_{pk}	S_{pk}	V_{pk}(SC)	S_{pk}(SC)	refs, epoch
(° °)	(h m s)	(° ′ ″)	(km s^{-1})		(km s^{-1})	(Jy)	(km s^{-1})	(Jy)	
G 20.081−0.135	18 28 10.32	−11 28 47.6	42.2	43.9	43.5	1.7	43.6	1.62	A2008aug23 (W98)
G 20.237+0.065	18 27 44.56	−11 14 54.2	68.1	77.9	71.9	84.9	71.9	86.22	M2005jan30 (Fuji14, C09, W98)
G 20.239+0.065	18 27 44.96	−11 14 47.9	59.6	71.0	70.4	6.9	70.9	6.59	M2005jan30 (C09, Fuji14)
G 20.364−0.013	18 28 15.91	−11 10 20.4	49.8	59.3	55.9	2.9	56.0	3.02	A2006dec04
G 20.733−0.059	18 29 07.99	−10 52 00.6	55.0	63.8	60.7	1.3	60.8	1.52	A2006dec04
G 20.926−0.050	18 29 27.79	−10 41 28.8	23.5	29.7	27.4	4.1	25.9	2.73	M2008feb20 (A2006dec04)
G 20.963−0.075	18 29 37.34	−10 40 12.6	33.6	34.8	34.6	2.2	34.6	2.27	M2008feb20 (A2006dec04)
G 21.023−0.063	18 29 41.55	−10 36 42.3	29.0	34.7	31.1	2.2	31.2	2.16	M2008feb20 (A2006dec04)
G 21.407−0.254	18 31 06.35	−10 21 38.4	82.7	95.3	89.0	14.5	89.0	13.01	A2006dec04 (Bart09)
G 21.562−0.033	18 30 36.07	−10 07 10.9	108.8	120.7	117.2	13.0	117.2	12.97	M2006dec17 (A2006dec04)
G 21.848−0.240	18 31 53.06	−09 57 45.4	81.3	83.8	81.9	0.7	82.0	0.93	M2008feb20
G 21.880+0.014	18 31 01.75	−09 49 00.5	16.6	21.6	20.3	5.5	20.4	5.36	A2014feb10 (W98)
G 22.039+0.222	18 30 34.70	−09 34 47.0	45.3	55.2	53.2	5.9	49.5	4.97	Cyg09 (A2006dec04)
G 22.335−0.155	18 32 29.41	−09 29 29.7	23.1	42.1	35.6	37.6	35.6	38.88	C09 (Bart09)
G 22.356+0.066	18 31 44.12	−09 22 12.3	75.2	89.6	80.1	12.3	80.2	12.92	Bart09 (W98)
G 22.435−0.169	18 32 43.82	−09 24 33.2	22.0	40.3	29.6	13.6	29.6	13.81	C09 (M2005jan30)
G 23.003+0.124	18 32 44.25	−08 46 10.7	109.0	114.2	110.5	2.4	110.7	2.47	A2006dec04
G 23.010−0.410	18 34 40.27	−09 00 38.3	68.0	87.5	74.4	582	74.8	482.60	C09 (M2005jan30, Cyg09, Xu09, Mos11)
G 23.126+0.395	18 31 59.75	−08 32 09.1	11.9	22.4	13.8	1.1	22.1	1.95	M2008feb20 (A2014feb09)
G 23.207−0.377	18 34 55.22	−08 49 15.0	72.3	85.5	77.0	37.1	81.7	41.15	M2005jan30 (Bart09, A2006dec04)
G 23.257−0.241	18 34 31.26	−08 42 46.7	58.4	66.5	63.9	6.4	64.1	8.53	A2014feb10 (W98)
G 23.365−0.291	18 34 54.13	−08 38 25.6	79.5	83.3	82.5	1.5	82.6	1.96	M2007apr19 (A2006dec04)
G 23.389+0.185	18 33 14.33	−08 23 57.7	71.9	77.6	75.4	48.3	74.6	39.07	M2005jan30 (Bart09)
G 23.437−0.184	18 34 39.27	−08 31 39.3	100.5	112.8	102.9	86.0	103.0	75.42	Fuji14 (A2006dec04, C09, W98)
G 23.440−0.182	18 34 39.18	−08 31 25.4	94.7	100.4	96.6	56.6	96.6	47.19	Brunth09 (Fuji14, C09, W98)
G 23.484+0.097	18 33 44.05	−08 21 20.6	81.4	93.5	87.0	8.8	87.2	9.33	W98 (A2014feb10)
G 23.657−0.127	18 34 51.56	−08 18 21.3	76.0	87.9	82.4	13.6	82.4	14.17	Bart09 (Niez05)
G 23.706−0.198	18 35 12.37	−08 17 39.4	58.1	81.8	78.7	15.7	79.1	11.74	Bart09 (W98)
G 23.885+0.060	18 34 36.84	−08 01 00.7	43.6	45.3	45.0	1.9	43.9	1.51	A2014feb09
G 23.901+0.077	18 34 34.92	−07 59 42.2	31.2	36.0	35.7	0.7	31.6	0.79	M2007apr09 (A2014feb09)
G 23.966−0.109	18 35 22.21	−08 01 22.5	66.9	75.1	70.9	20.0	70.9	18.64	Bart09 (Niez05, Cyg09)
G 23.986−0.089	18 35 20.09	−07 59 45.0	63.8	67.1	65.1	1.5	65.1	2.54	Cyg09
G 23.996−0.100	18 35 23.49	−07 59 29.8	65.9	68.6	68.2	1.7	68.2	3.02	Cyg09
G 24.148−0.009	18 35 20.94	−07 48 55.7	16.4	19.8	17.4	41.9	17.5	27.11	Bart09 (Niez05, Xu09)
G 24.329+0.144	18 35 08.09	−07 35 03.6	107.1	120.1	110.3	8.0	110.2	5.67	C09 (X09)
G 24.461+0.198	18 35 11.33	−07 26 31.1	112.2	126.6	125.5	3.6	125.1	3.73	M2007apr17
G 24.493−0.039	18 36 05.83	−07 31 20.6	106.8	116.9	115.2	8.8	115.2	11.45	C09
G 24.541+0.312	18 34 55.72	−07 19 06.7	103.6	110.6	106.5	9.6	105.6	35.99	Bart09 (Niez05)
G 24.634−0.324	18 37 22.71	−07 31 42.1	33.8	50.8	35.6	5.7	43.9	4.20	Bart09
G 24.676−0.150	18 36 49.97	−07 24 42.1	103.5	116.9	116.1	3.8	116.3	4.18	M2009feb14
G 24.790+0.083a	18 36 12.56	−07 12 11.3	106.0	116.8	113.3	119.6	113.4	115.46	A2014feb09 (M2005jan30, W98, Mos07)
G 24.790+0.083b	18 36 12.47	−07 12 10.5	109.2	112.8	110.4	28.2	110.4	28.16	A2014feb09 (M2005jan30, Mos07)
G 24.790+0.084	18 36 12.30	−07 12 10.4	102.2	105.6	102.4	0.6	102.6	0.84	A2014feb09
G 24.791+0.082	18 36 13.13	−07 12 08.2	103.0	107.3	105.8	0.8	105.8	1.50	A2014feb09
G 24.850+0.087	18 36 18.40	−07 08 51.0	107.4	116.0	110.0	15.0	110.0	17.22	M2005jan30 (A2014feb09, W98)
G 24.920+0.088	18 36 25.94	−07 05 07.8	50.2	53.7	53.3	4.7	53.3	7.64	M2008apr11 (Cyg09)
G 24.943+0.074	18 36 31.56	−07 04 16.8	45.2	48.5	46.6	1.7	46.7	3.07	M2008apr11 (Cyg09)
G 25.226+0.288	18 36 16.97	−06 43 18.3	41.6	42.4	42.0	2.0	42.1	3.23	M2007mar30
G 25.270−0.434	18 38 56.96	−07 00 49.2	52.0	67.3	65.9	2.7	65.9	1.96	Cyg09
G 25.382−0.182	18 38 15.20	−06 47 56.2	56.8	59.0	58.2	5.7	58.2	2.76	M2009feb14
G 25.407−0.170	18 38 15.52	−06 46 16.7	59.4	62.7	60.8	2.2	60.7	2.66	M2007mar09
G 25.411+0.105	18 37 16.92	−06 38 30.5	93.0	97.8	97.1	12.7	97.2	19.63	M2008feb20 (Bart09, Beu02)
G 25.494+0.062	18 37 35.44	−06 35 13.4	92.1	107.0	103.8	1.6	103.8	1.83	M2007mar02
G 25.613+0.226	18 37 13.42	−06 24 24.2	107.2	115.1	110.1	0.3	109.8	0.78	A2014feb09
G 25.650+1.049	18 34 20.90	−05 59 42.2	38.2	43.8	41.7	120.5	41.9	72.33	M2008apr11 (A2014feb10, W98)
G 25.710+0.044	18 38 03.15	−06 24 14.9	89.0	103.5	95.6	546.3	95.6	607.00	A2014feb10 (W98, Fuji14)

Table 1 – *continued*

Source name	Equatorial coordinates		Velocity range		MX/ATCA data		Survey cube data		Position
(l, b)	RA (2000)	Dec. (2000)	V_L	V_H	V_{pk}	S_{pk}	V_{pk}(SC)	S_{pk}(SC)	refs, epoch
(° °)	(h m s)	(° ′ ″)	(km s^{-1})		(km s^{-1})	(Jy)	(km s^{-1})	(Jy)	
G 25.826−0.178	18 39 03.63	−06 24 09.7	84.7	99.9	91.7	73.6	91.6	70.82	A2014feb10 (W98, Fuji14)
G 25.838−0.378	18 39 47.88	−06 29 00.9	− 2.7	− 0.3	− 1.6	0.8	− 1.8	0.79	A2014feb09
G 25.920−0.141	18 39 06.07	−06 18 04.7	111.6	114.9	114.8	1.2	113.9	1.55	M2006dec18
G 26.422+1.685	18 33 30.51	−05 01 02.0	27.3	31.7	31.0	3.8	31.1	2.84	M2007apr09
G 26.545+0.423	18 38 14.46	−05 29 16.8	82.3	82.7	82.5	1.2	82.3	1.34	M2007mar09
G 26.527−0.267	18 40 40.26	−05 49 12.9	102.4	110.0	104.2	1.2	109.6	3.19	M2006dec18
G 26.598−0.024	18 39 55.93	−05 38 44.6	16.7	28.4	24.9	11.6	24.9	14.67	Bart09 (Beu02)
G 26.601−0.221	18 40 38.57	−05 44 01.6	102.2	116.3	103.4	13.5	103.4	18.65	M2008apr09
G 26.648+0.018	18 39 52.68	−05 34 54.6	103.7	114.5	109.4	0.8	107.7	2.20	A2014feb09
G 27.011−0.039	18 40 44.88	−05 17 09.8	− 22.1	− 17.7	− 18.3	1.2	− 21.0	2.12	M2007apr09
G 27.221+0.136	18 40 30.55	−05 01 05.4	105.1	121.0	118.6	14.8	118.7	27.80	Bart09
G 27.220+0.261	18 40 03.69	−04 57 42.4	6.2	18.5	9.2	6.8	9.2	8.67	A2014feb09 (Xu09)
G 27.286+0.151	18 40 34.51	−04 57 14.4	23.4	36.7	34.8	32.4	34.8	38.32	M2008feb20
G 27.365−0.166	18 41 51.06	−05 01 43.5	87.6	104.0	99.8	31.8	100.2	46.03	M2009feb07 (Xu09)
G 27.500+0.107	18 41 07.38	−04 47 02.3	79.8	88.0	87.3	1.5	87.3	0.91	M2007mar09
G 27.757+0.050	18 41 47.99	−04 34 52.6	92.3	105.4	99.2	0.8	99.1	1.77	A2014feb09
G 27.783−0.259	18 42 56.96	−04 41 59.0	96.2	106.3	98.3	4.7	98.2	3.93	M2008apr09
G 27.784+0.057	18 41 49.58	−04 33 13.8	108.2	113.3	111.8	2.2	108.5	3.03	A2014feb09 (M2006dec17)
G 27.869−0.235	18 43 01.55	−04 36 43.1	19.9	20.3	20.1	0.3	20.1	0.40	A2014feb09
G 28.011−0.426	18 43 57.96	−04 34 21.9	15.6	28.5	16.9	5.5	16.9	10.07	A2014feb09 (M2007jan26)
G 28.146−0.005	18 42 42.59	−04 15 36.5	91.6	104.9	101.2	39.1	101.2	58.09	C09 (W98)
G 28.201−0.049	18 42 58.08	−04 13 56.2	93.9	102.2	97.3	2.6	97.3	2.72	C09 (W98)
G 28.282−0.359	18 44 13.26	−04 18 04.9	40.5	43.1	40.9	3.1	40.9	2.90	M2006apr01 (Cyg09, A2014feb10)
G 28.305−0.387	18 44 21.99	−04 17 38.4	79.7	94.5	81.8	44.2	81.6	72.80	W98 (A2014feb10)
G 28.321−0.011	18 43 03.11	−04 06 26.4	96.7	106.2	104.8	2.4	103.6	2.06	M2006apr17 (A2006apr01)
G 28.397+0.081	18 42 51.98	−03 59 53.6	68.2	82.4	71.5	16.4	71.5	12.98	A2014feb09
G 28.523+0.127	18 42 55.89	−03 51 55.4	38.8	39.7	39.6	1.5	39.4	0.95	M2008apr11
G 28.532+0.129	18 42 56.50	−03 51 21.6	23.7	28.7	27.0	1.5	27.4	2.41	A2014feb09
G 28.608+0.018	18 43 28.52	−03 50 22.8	99.7	107.9	106.4	3.7	106.4	3.46	M2006apr17 (A2006apr01)
G 28.687−0.283	18 44 41.54	−03 54 22.1	89.9	92.7	92.3	3.1	92.4	1.20	A2006apr01
G 28.700+0.406	18 42 15.57	−03 34 46.9	87.9	95.7	94.2	0.6	94.3	1.58	M2007jan26
G 28.817+0.365	18 42 37.35	−03 29 41.0	86.4	93.2	90.6	6.2	90.7	8.06	M2009feb07 (Bart09)
G 28.832−0.253	18 44 51.09	−03 45 48.7	79.5	93.8	83.6	63.5	83.5	83.77	M2008apr09 (Cyg09, W98)
G 28.842+0.493	18 42 12.54	−03 24 51.1	79.3	89.7	83.2	2.0	83.2	3.98	A2014feb09
G 28.848−0.228	18 44 47.46	−03 44 17.2	99.8	103.6	102.8	1.8	102.8	2.35	M2008apr09 (Cyg09, W98)
G 28.861+0.065	18 43 46.24	−03 35 33.4	104.7	105.5	105.3	0.8	105.2	0.77	A2014feb09
G 29.320−0.162	18 45 25.16	−03 17 16.9	40.4	50.3	48.9	3.6	48.9	8.50	M2008apr11
G 29.603−0.625	18 47 35.41	−03 14 50.1	80.2	82.4	80.5	1.3	81.5	2.04	M2006apr12 (A2006apr01)
G 29.863−0.044	18 45 59.57	−02 45 04.4	98.8	105.2	101.4	83.9	101.4	79.98	Xu09 (W98)
G 29.955−0.016	18 46 03.74	−02 39 22.2	93.4	106.4	96.0	169.5	96.0	238.15	M2009feb07 (Minier01, W98)
G 29.978−0.047	18 46 12.96	−02 39 01.4	96.5	106.2	96.9	33.0	103.0	37.26	M2006dec17
G 29.993−0.282	18 47 04.82	−02 44 39.8	102.9	103.8	103.2	1.7	103.0	2.60	M2006apr18 (A2006apr01)
G 30.010−0.273	18 47 04.71	−02 43 31.2	105.9	106.3	106.1	2.7	106.1	2.24	M2006apr18 (A2006apr01)
G 30.198−0.169	18 47 03.04	−02 30 36.4	100.4	111.1	108.2	18.0	108.6	35.50	A2014mar15 (Xu09)
G 30.225−0.180	18 47 08.30	−02 29 28.9	109.8	115.0	113.2	19.4	113.4	14.20	A2014mar15 (Xu09)
G 30.317+0.070	18 46 25.03	−02 17 41.0	30.4	51.3	36.2	7.5	36.5	14.70	M2006apr01 (Bart09)
G 30.370+0.482	18 45 02.72	−02 03 33.7	12.2	19.7	12.4	1.8	19.5	1.92	M2006apr11 (A2006apr01)
G 30.400−0.296	18 47 52.31	−02 23 16.0	96.5	106.0			98.3	5.44	A2014mar15 (Bart09)
G 30.419−0.232	18 47 40.76	−02 20 30.1	102.1	111.3	102.9	13.4	103.0	26.55	M2006apr18 (A2006apr01)
G 30.423+0.466	18 45 12.08	−02 01 13.6	5.1	9.1	7.5	1.4	8.0	1.98	M2006apr15 (A2006apr01)
G 30.542+0.011	18 47 02.26	−02 07 17.7	51.7	54.8	53.1	0.5	53.2	0.95	M2008apr11
G 30.58−0.14†	*18 47 39.2*	*−02 09 19*	115.2	116.2	115.5	0.3	115.5	0.44	–
G 30.589−0.043	18 47 18.86	−02 06 17.2	36.5	49.0	43.0	5.9	43.1	7.10	A2014mar15 (W98)
G 30.703−0.068	18 47 36.82	−02 00 53.8	85.4	92.8	88.2	128.5	88.2	131.40	A2014mar15 (W98)
G 30.760−0.052	18 47 39.78	−01 57 23.4	85.8	94.9	91.7	56.0	91.7	60.22	A2014mar15 (W98)
G 30.771−0.804	18 50 21.55	−02 17 24.0	73.7	76.7	74.4	7.4	74.4	10.10	M2006apr12
G 30.780+0.230	18 46 41.52	−01 48 37.1	47.4	49.3	48.9	44.1	49.0	57.02	A2014mar15 (W98)
G 30.788+0.204	18 46 48.09	−01 48 53.9	74.2	89.9	84.5	19.7	84.5	22.02	M2006apr12 (W98)
G 30.774+0.078	18 47 13.39	−01 53 04.1	98.2	99.4	98.4	0.8	98.4	0.79	M2007mar02 (A2006apr01)
G 30.818−0.057	18 47 46.97	−01 54 26.4	99.3	110.2	101.3	9.5	108.3	9.52	M2006apr18 (W98)
G 30.818+0.273	18 46 36.60	−01 45 22.7	100.0	110.4	104.8	2.3	104.8	2.90	M2008apr09
G 30.822−0.053	18 47 46.53	−01 54 07.4	90.7	96.1	93.2	8.7	93.1	9.16	M2006apr18

Table 1 – *continued*

Source name	Equatorial coordinates		Velocity range		MX/ATCA data		Survey cube data		Position
(l, b)	RA (2000)	Dec. (2000)	V_L	V_H	V_{pk}	S_{pk}	V_{pk}(SC)	S_{pk}(SC)	refs, epoch
(° °)	(h m s)	(° ′ ″)	(km s^{-1})		(km s^{-1})	(Jy)	(km s^{-1})	(Jy)	
G 30.851+0.123	18 47 12.26	−01 47 46.6	27.3	37.7	27.5	0.9	29.0	1.47	M2006apr11 (A2006apr01)
G 30.898+0.161	18 47 09.13	−01 44 11.1	98.4	111.4	101.8	67.2	101.8	76.98	A2014mar15 (W98, Xu09)
G 30.960+0.086	18 47 32.00	−01 42 57.6	35.8	40.5	40.1	0.7	39.8	1.60	A2014mar15
G 30.972−0.142	18 48 22.07	−01 48 30.3	73.7	80.5	77.8	16.3	77.9	25.82	A2014mar15
G 30.973+0.562	18 45 51.69	−01 29 13.3	19.6	20.5	19.9	0.7	19.9	0.95	M2006apr11 (A2006apr01)
G 30.980+0.216	18 47 06.47	−01 38 20.0	107.4	111.5	111.0	2.4	111.2	2.38	M2006apr18 (A2006apr01)
G 31.047+0.356	18 46 43.86	−01 30 54.2	73.7	84.2	83.0	5.0	80.9	4.40	Bart09
G 31.059+0.093	18 47 41.35	−01 37 26.2	14.8	20.5	16.5	19.7	16.5	23.83	A2014mar15 (W98)
G 31.076+0.457	18 46 25.44	−01 26 33.5	25.1	27.2	25.5	0.7	26.8	1.15	M2006apr11 (A2006apr01)
G 31.122+0.063	18 47 54.68	−01 34 56.9	47.3	48.4	48.0	2.2	48.1	2.85	A2014mar15 (A2006apr01)
G 31.158+0.046	18 48 02.40	−01 33 26.8	40.5	43.6	41.1	1.8	41.2	4.35	A2014mar15 (Bart09)
G 31.182−0.148	18 48 46.41	−01 37 28.1	43.2	52.3	46.3	2.0	46.3	3.07	M2006apr01 (A2006apr01)
G 31.281+0.061	18 48 12.43	−01 26 30.1	102.0	114.1	110.3	70.6	110.4	131.40	A2014mar15 (W98)
G 31.412+0.307	18 47 34.29	−01 12 45.6	89.9	106.8	95.8	15.4	95.8	22.28	Mos13 (W98)
G 31.581+0.077	18 48 41.94	−01 10 02.5	91.5	100.2	98.9	5.6	98.9	9.60	Bart09
G 31.594−0.192	18 49 40.89	−01 16 43.1	46.7	48.5	48.3	1.2	48.2	1.84	M2006apr01 (A2006apr01)
G 32.045+0.059	18 49 36.56	−00 45 45.9	91.8	102.3	92.8	105.1	92.9	163.30	M2008feb16
G 32.082+0.078	18 49 36.60	−00 43 16.4	90.6	103.8	92.9	9.7	97.7	4.61	M2008feb16
G 32.516+0.323	18 49 31.74	−00 13 20.8	52.2	53.0	52.5	1.6	52.4	2.06	M2006apr01 (A2006apr01)
G 32.744−0.075	18 51 21.87	−00 12 05.0	24.5	44.3	38.5	56.8	38.5	59.63	A2014mar15 (M2005jan30)
G 32.802+0.193	18 50 30.98	−00 01 39.0	26.2	28.1	27.2	1.2	27.5	1.04	M2006apr11
G 32.825−0.328	18 52 24.69	−00 14 39.7	81.5	84.2	82.4	1.6	82.3	1.65	M2006apr12
G 32.914−0.096	18 51 44.69	−00 03 35.5	103.2	104.2	103.5	0.7	103.6	1.00	M2008feb16
G 32.963−0.340	18 52 42.35	−00 07 39.1	44.4	50.0	46.7	0.3	48.7	0.83	M2008feb16
G 32.992+0.034	18 51 25.58	+00 04 08.3	82.9	94.7	91.9	11.5	91.9	18.18	Bart09
G 33.093−0.073	18 51 59.58	+00 06 35.5	94.4	106.5	103.9	16.9	103.9	19.90	A2014mar15
G 33.133−0.092	18 52 07.82	+00 08 12.8	68.7	81.9	73.2	12.6	73.2	16.93	A2014mar15
G 33.317−0.360	18 53 25.30	+00 10 43.9	25.7	31.5	–	–	31.2	1.62	M2006apr11
G 33.393+0.010	18 52 14.62	+00 24 52.9	96.3	107.7	105.2	18.8	105.3	23.71	A2014mar15
G 33.486+0.040	18 52 18.39	+00 30 40.2	101.8	123.9	121.7	3.3	122.8	3.93	M2006apr15
G 33.641−0.228	18 53 32.56	+00 31 39.3	56.9	64.2	60.3	138.4	59.6	155.00	A2014mar15 (Bart09)
G 33.634−0.021	18 52 47.56	+00 36 54.2	102.7	104.2	103.1	0.7	103.6	0.84	M2006apr18
G 33.725−0.120	18 53 18.78	+00 39 05.0	52.8	60.8	54.1	3.3	53.4	3.28	A2014mar15
G 33.852+0.018	18 53 03.09	+00 49 36.5	60.5	65.0	61.0	2.4	64.1	3.38	A2014mar15
G 33.980−0.019	18 53 25.02	+00 55 26.0	58.6	65.9	59.0	3.3	58.9	5.43	Bart09
G 34.096+0.018	18 53 29.94	+01 02 39.4	54.6	61.58	56.1	6.2	56.0	5.56	A2014mar15
G 34.244+0.133	18 53 21.44	+01 13 44.4	54.4	63.5	54.9	5.0	55.3	7.31	A2014mar15
G 34.257+0.153	18 53 18.63	+01 14 57.4	55.9	62.2	57.6	22.8	57.6	26.27	M2005jan31 (2014mar15)
G 34.267−0.210	18 54 37.25	+01 05 33.7	48.1	55.1	54.5	8.2	54.6	8.14	M2008feb16
G 34.396+0.222	18 53 19.08	+01 24 13.8	55.2	63.4	55.7	17.6	55.7	11.00	A2014mar15
G 34.751−0.093	18 55 05.22	+01 34 36.3	50.1	54.2	53.2	4.4	52.8	4.74	Bart09 (A2014mar15)
G 34.757+0.025	18 54 40.74	+01 38 06.4	74.8	77.3	76.5	1.8	76.5	1.88	M2008feb16
G 34.791−1.387	18 59 45.98	+01 01 19.0	43.1	49.6	46.9	15.5	47.0	24.49	M2008feb16
G 34.82+0.35†	*18 53 37.8*	*+01 50 13*	59.3	60.0	59.8	0.2	59.7	0.71	–
G 35.025+0.350	18 54 00.66	+02 01 19.2	41.1	47.0	44.4	25.9	44.4	24.80	Pan11 (Cyg09)
G 35.132−0.744	18 58 06.14	+01 37 07.5	26.5	39.1	35.4	48.4	35.4	84.28	M2009feb14
G 35.197−0.743	18 58 13.05	+01 40 35.7	28.0	29.0	28.6	172.2	28.5	174.00	M2009feb14 (Xu09)
G 35.197−0.743n	18 58 12.95	+01 40 37.5	26.1	37.0	29.9	55.2	29.9	57.97	M2009feb14
G 35.200−1.736	19 01 45.54	+01 13 32.6	39.4	47.0	44.5	519.9	42.5	965.20	M2008feb16
G 35.247−0.237	18 56 30.39	+01 57 08.9	72.0	73.4	72.4	1.5	72.4	1.68	Pan11
G 35.397+0.025	18 55 50.78	+02 12 19.1	88.9	89.5	89.2	0.8	89.0	1.48	Pan11
G 35.588+0.060	18 56 04.22	+02 23 28.3	43.9	52.2	44.1	0.4	45.2	0.71	Pan11
G 35.793−0.175	18 57 16.89	+02 27 58.1	56.0	64.8	60.7	17.7	60.8	23.11	Pan11 (Bart09, Niez05)
G 36.115+0.552	18 55 16.79	+03 05 05.4	69.6	84.8	73.1	39.7	73.0	29.25	Bart09 (Niez05)
G 36.634−0.203	18 58 55.24	+03 12 04.7	77.2	78.8	77.4	1.1	77.4	1.03	Pan11
G 36.705+0.096	18 57 59.12	+03 24 06.1	52.0	63.0	53.1	5.4	53.1	7.14	Pan11 (Bart09)
G 36.839−0.022	18 58 39.21	+03 28 00.9	53.1	64.3	61.6	3.0	61.7	2.55	Pan11
G 36.918+0.483	18 56 59.79	+03 46 03.6	−36.4	−35.5	−35.9	1.2	−35.9	1.21	Pan11

Table 1 – *continued*

Source name	Equatorial coordinates		Velocity range		MX/ATCA data		Survey cube data		Position
(l, b)	RA (2000)	Dec. (2000)	V_L	V_H	V_{pk}	S_{pk}	V_{pk}(SC)	S_{pk}(SC)	refs, epoch
(° °)	(h m s)	(° ′ ″)	(km s^{-1})		(km s^{-1})	(Jy)	(km s^{-1})	(Jy)	
G 37.030−0.038	18 59 03.64	+03 37 45.1	78.0	79.5	78.6	7.3	78.5	9.56	Pan11 (Bart09)
G 37.043−0.035	18 59 04.41	+03 38 32.8	79.0	85.9	80.2	8.2	80.2	8.14	Pan11
G 37.430+1.518	18 54 14.23	+04 41 41.1	40.2	52.7	41.2	395.1	41.2	336.10	M2008feb16
G 37.479−0.105	19 00 07.14	+03 59 53.1	53.8	63.7	62.5	8.1	54.7	10.02	Pan11 (Bart09, Cyg09)
G 37.546−0.112	19 00 16.06	+04 03 16.1	49.3	52.8	52.5	4.1	50.0	5.01	Pan11 (Cyg09)
G 37.554+0.201	18 59 09.99	+04 12 15.5	78.4	91.7	83.7	7.9	83.8	14.71	Pan11
G 37.598+0.425	18 58 26.80	+04 20 45.5	84.8	94.6	87.0	14.2	87.0	19.77	Pan11 (Bart09)
G 37.735−0.112	19 00 36.84	+04 13 20.0	50.0	51.0	50.3	1.0	50.3	1.02	Pan11
G 37.753−0.189	19 00 55.42	+04 12 12.6	54.4	65.4	54.6	1.5	54.8	1.71	Pan11 (Bart14)
G 37.767−0.214	19 01 02.27	+04 12 16.6	68.9	69.2	–	–	69.0	0.50	Pan11
G 38.037−0.300	19 01 50.47	+04 24 18.9	54.7	67.1	58.2	8.8	58.2	10.45	Pan11 (Bart09)
G 38.119−0.229	19 01 44.15	+04 30 37.4	67.2	80.1	70.3	3.6	70.3	2.65	Pan11
G 38.203−0.067	19 01 18.73	+04 39 34.3	77.8	85.3	84.2	10.4	84.3	10.13	Pan11 (Bart09)
G 38.255−0.200	19 01 52.96	+04 38 39.5	65.4	73.3	73.1	0.6	70.2	0.98	Pan11
G 38.258−0.074	19 01 26.23	+04 42 17.3	6.0	15.9	15.5	8.0	15.4	8.01	Pan11 (M2007jan27)
G 38.565+0.538	18 59 49.13	+05 15 28.9	− 30.0	− 27.2	− 28.8	1.6	− 28.8	1.50	M2009feb12
G 38.598−0.212	19 02 33.46	+04 56 36.4	62.3	69.3	62.5	0.4	62.4	0.56	Pan11
G 38.653+0.088	19 01 35.24	+05 07 47.4	− 31.6	− 28.5	− 31.4	1.3	− 31.4	1.63	Pan11
G 38.916−0.353	19 03 38.66	+05 09 42.5	30.9	33.9	32.0	2.7	32.0	2.78	Pan11
G 39.100+0.491	19 00 58.04	+05 42 43.9	12.1	30.2	15.9	20.3	15.9	22.57	Bart09 (Niez05, Cyg09)
G 39.388−0.141	19 03 45.31	+05 40 42.7	58.7	69.5	60.5	0.7	60.4	1.34	Pan11
G 40.282−0.219	19 05 41.22	+06 26 12.7	64.8	84.6	74.0	23.0	74.0	22.83	Pan11 (A2014feb09, Bart14)
G 40.425+0.700	19 02 39.62	+06 59 09.0	3.3	17.0	15.6	22.6	15.6	22.28	M2009feb14 (C09, Bart14)
G 40.597−0.719	19 08 03.29	+06 29 12.9	72.2	76.6	76.2	1.1	72.7	0.85	M2009feb18
G 40.622−0.138	19 06 01.63	+06 46 36.2	29.3	37.0	31.1	11.5	31.2	12.57	Pan11 (C09)
G 40.934−0.041	19 06 15.38	+07 05 54.5	36.4	41.5	36.6	2.4	36.7	2.60	Pan11
G 41.075−0.125	19 06 49.05	+07 11 06.6	57.2	57.8	–	–	57.6	0.80	Pan11
G 41.121−0.107	19 06 50.25	+07 14 01.5	35.5	37.4	36.6	0.6	36.5	0.84	Pan11
G 41.123−0.220	19 07 14.86	+07 11 00.7	55.3	64.2	63.4	2.6	63.5	2.60	Pan11 (Bart14)
G 41.156−0.201	19 07 14.37	+07 13 18.1	55.8	63.8	56.0	1.2	61.8	1.66	Pan11 (Bart14)
G 41.226−0.197	19 07 21.38	+07 17 08.2	54.6	63.4	57.3	5.4	55.5	5.58	Pan11 (Bart14)
G 41.348−0.136	19 07 21.84	+07 25 17.3	6.7	14.8	11.8	17.7	11.8	16.06	Pan11 (Bart14)
G 42.034+0.190	19 07 28.19	+08 10 53.5	7.0	17.8	12.9	21.8	12.9	23.87	Pan11
G 42.13+0.52†	*19 06 28.9*	*+08 25 10*	− 33.6	− 32.9	− 33.3	0.5	− 33.4	0.86	–
G 42.304−0.299	19 09 43.59	+08 11 41.4	26.2	30.7	28.2	5.3	28.2	5.92	Pan11
G 42.435−0.260	19 09 49.86	+08 19 45.4	65.8	68.8	66.8	2.6	66.8	2.00	Pan11
G 42.698−0.147	19 09 55.07	+08 36 53.5	− 47.1	− 39.1	− 42.8	3.7	− 42.9	3.30	Pan11
G 43.038−0.453	19 11 38.98	+08 46 30.7	54.3	63.9	54.8	6.2	54.9	6.95	Pan11
G 43.074−0.077	19 10 22.05	+08 58 51.5	9.8	11.2	10.2	7.6	10.3	8.83	Pan11
G 43.149+0.013	19 10 11.05	+09 05 20.5	12.8	14.4	13.2	16.2	13.0	13.42	Pan11 (C09, Bart14, Xu09)
G 43.165+0.013	19 10 12.88	+09 06 12.2	6.2	22.5	9.3	28.7	9.3	31.34	Pan11 (C09, Bart 14)
G 43.167−0.004	19 10 16.72	+09 05 51.3	− 1.4	− 0.5	− 1.2	2.2	− 1.2	2.59	Pan11 (C09, Bart14)
G 43.171+0.005	19 10 15.36	+09 06 15.5	18.0	22.6	18.9	18.9	18.9	18.32	Pan11 (C09, Bart14)
G 43.175−0.015	19 10 20.07	+09 05 55.9	12.3	12.7	12.6	0.5	11.2	1.19	Pan11
G 43.180−0.518	19 12 09.02	+08 52 14.3	55.6	65.6	58.9	3.4	58.9	2.21	M2008feb18
G 43.795−0.127	19 11 53.99	+09 35 50.6	39.4	44.1	39.7	37.3	39.7	46.47	Pan11 (C09)
G 43.890−0.784	19 14 26.39	+09 22 36.6	42.9	58.0	51.9	9.6	47.6	10.16	M2008feb18 (Xu09)
G 44.310+0.041	19 12 15.82	+10 07 53.5	55.2	56.5	55.8	0.5	55.7	0.91	Pan11
G 44.644−0.516	19 14 53.77	+10 10 07.7	49.0	49.9	49.6	0.5	49.5	1.10	Pan11
G 45.071+0.132	19 13 22.13	+10 50 53.1	57.4	58.4	57.7	6.6	57.8	46.86	Pan11
G 45.380−0.594	19 16 34.14	+10 47 01.6	52.7	53.9	53.3	3.0	53.3	2.34	M2008feb18
G 45.445+0.069	19 14 18.29	+11 08 59.0	49.2	50.7	49.8	1.5	49.9	1.04	Pan11(C09)
G 45.467+0.053	19 14 24.15	+11 09 43.4	55.6	59.3	56.0	1.5	56.0	5.07	Pan11 (C09, Bart14)
G 45.473+0.134	19 14 07.36	+11 12 16.0	59.5	73.4	65.7	4.6	65.7	5.80	M2008feb18 (2014feb09, C09, Bart14)
G 45.493+0.126	19 14 11.36	+11 13 06.4	56.9	58.1	57.1	7.8	57.2	7.65	M2008feb18 (Pan11, A2014feb09, C09, Bart14)
G 45.804−0.356	19 16 31.08	+11 16 12.0	54.9	71.1	59.9	11.7	59.1	15.70	Pan11
G 46.066+0.220	19 14 56.08	+11 46 13.0	22.6	24.2	23.5	1.0	23.4	0.98	Pan11
G 46.115+0.387	19 14 25.52	+11 53 26.0	57.6	62.7	58.3	1.2	59.1	1.21	Pan11
G 48.902−0.273	19 22 10.33	+14 02 43.5	71.1	72.5	71.8	0.5	71.9	0.89	Pan11
G 48.990−0.299	19 22 26.13	+14 06 39.8	71.1	72.3	71.5	0.6	71.6	1.03	Pan11
G 49.043−1.079	19 25 22.25	+13 47 19.5	34.9	41.2	36.6	35.3	36.7	31.28	M2008feb18

Table 1 – *continued*

Source name	Equatorial coordinates		Velocity range		MX/ATCA data		Survey cube data		Position
(l, b)	RA (2000)	Dec. (2000)	V_L	V_H	V_{pk}	S_{pk}	V_{pk}(SC)	S_{pk}(SC)	refs, epoch
(° °)	(h m s)	(° ′ ″)	(km s^{-1})		(km s^{-1})	(Jy)	(km s^{-1})	(Jy)	
G 49.265+0.311	19 20 44.86	+14 38 26.9	− 6.6	7.4	− 4.7	7.4	− 4.6	7.59	Pan11
G 49.349+0.413	19 20 32.45	+14 45 45.4	66.3	69.1	68.0	8.1	68.1	10.06	Pan11
G 49.416+0.326	19 20 59.21	+14 46 49.7	− 15.6	− 9.8	− 12.0	8.0	− 12.0	9.45	Pan11 (Xu09, Cyg09)
G 49.417+0.324	19 20 59.82	+14 46 49.1	− 26.9	− 23.8	− 26.6	2.7	− 25.6	3.38	Pan11 (Cyg09)
G 49.470−0.371	19 23 37.90	+14 29 59.3	63.5	76.1	63.8	5.7	63.9	6.67	Pan11 (C09)
G 49.471−0.369	19 23 37.60	+14 30 05.4	72.0	74.2	73.5	1.7	73.6	1.47	C09
G 49.482−0.402	19 23 46.19	+14 29 47.1	44.5	52.0	51.8	36.5	51.8	28.27	Pan11 (C09)
G 49.489−0.369	19 23 39.82	+14 31 04.9	55.0	62.0	56.2	31.2	56.1	36.37	Pan11 (C09)
G 49.490−0.388	19 23 43.95	+14 30 34.5	51.0	62.0	59.2	852.1	59.3	794.30	Pan11 (C09, Xu09,Fuji14)
G 49.599−0.249	19 23 26.61	+14 40 17.0	60.8	66.8	63.1	31.4	63.0	48.95	Pan11
G 49.617−0.360	19 23 52.81	+14 38 03.3	49.9	50.7	50.4	0.5	50.2	0.81	Pan11
G 50.035+0.582	19 21 15.45	+15 26 49.2	− 10.5	− 2.4	− 5.1	4.0	− 5.1	5.75	M2009feb14
G 50.315+0.676	19 21 27.47	+15 44 18.6	25.6	32.2	30.1	3.5	30.1	3.22	M2008feb18
G 50.779+0.152	19 24 17.41	+15 54 01.6	48.2	50.4	49.1	3.9	49.1	4.72	Pan11
G 51.679+0.719	19 23 58.87	+16 57 41.8	− 3.8	8.6	7.3	1.0	7.2	1.22	Beu02 (2014feb09)
G 51.818+1.250	19 22 17.95	+17 20 06.5	46.0	47.0	46.5	1.9	46.5	2.19	M2008feb18
G 52.199+0.723	19 24 59.84	+17 25 17.9	1.7	4.5	3.7	6.3	3.8	4.82	M2008jul26
G 52.663−1.092	19 32 36.08	+16 57 38.5	56.0	68.2	65.9	4.6	65.2	2.45	M2008feb18 (Xu09)
G 52.922+0.414	19 27 34.96	+17 54 38.1	38.5	45.2	39.1	4.2	39.1	4.77	Pan11
G 53.036+0.113	19 28 55.49	+17 52 03.1	9.6	10.4	10.2	1.5	10.2	1.68	Pan11
G 53.142+0.071	19 29 17.58	+17 56 23.2	23.6	25.2	24.6	1.5	24.6	1.04	Pan11
G 53.618+0.035	19 30 23.02	+18 20 26.7	17.8	19.3	19.0	7.8	19.0	11.49	Pan11
G 56.963−0.235	19 38 17.10	+21 08 05.4	29.6	30.5	29.9	0.6	29.9	1.11	M2008jul26
G 57.610+0.025	19 38 40.74	+21 49 32.7	28.9	40.2	38.9	9.4	38.9	10.23	M2008jul26
G 58.775+0.644	19 38 49.13	+23 08 40.2	29.6	36.6	33.3	5.6	33.3	6.30	M2008jul26
G 59.634−0.192	19 43 50.00	+23 28 38.8	29.2	30.5	–	–	29.6	4.90	A2014feb09
G 59.783+0.065	19 43 11.25	+23 44 03.3	13.3	27.9	–	–	27.0	37.22	Bart14 (Xu09)
G 59.833+0.672	19 40 59.33	+24:04:46.5	35.7	39.8	–	–	38.2	24.29	A2014feb09

present in the literature), derived from instruments such as the ATCA, MERLIN, VLA and the European VLBI Network (EVN). These positions mostly show excellent coincidence. We do note, however, that while the methanol maser positions of Walsh et al. (1998) are mostly accurate, there are a number of sources within this longitude range that have an ∼7 arcsec offset in declination, likely owing to the east–west ATCA array used in the observations and the proximity of sources to a declination of zero degrees. In our own observations we opted for a hybrid array (not available to Walsh et al. 1998) to observe sources close to declination zero, giving us a large beam, but less elongation in declination and superior *uv*-coverage. This guards against position uncertainties to a large extent; however, we estimate that some of our ATCA positions for sources close to declination zero and the most northerly sources (meaning that they were necessarily observed at low elevations) could be as high as 1.5 arcsec in the most extreme cases. The majority of sources with positions derived from the ATCA will be accurate to our usually quoted positional uncertainty of 0.4 arcsec. Sources positioned with MERLIN are expected to have uncertainties better than (50, 100) mas for the majority, increasing to a few hundred milliarcseconds for sources South of ∼5° declination, sources observed in poor weather or sources that are particularly weak.

The integrated flux density of each of the masers has not been included in previous MMB catalogue papers. This parameter can be exploited in studies of masers, often regarded as being a slightly more robust measurement than peak flux density which can be more susceptible to temporal variability. In their study of the 12.2-GHz counterparts to the MMB masers, Breen et al. (2011, 2012b) have used the 6668-MHz integrated flux density (together with the 12.2-GHz integrated flux density) to investigate changes that occur alongside the evolution of the emission. Due to this, the integrated flux densities of the MMB sources have been presented in each of the 12.2-GHz methanol maser catalogue releases (Breen et al. 2012a,b, 2014) which cover the full MMB range with the exception of this current catalogue region (i.e. 186°–20° longitude). We have collated these data and present the 6668-MHz integrated flux densities of the full MMB survey region (including the current longitude range for the first time) in Table A1. de Villiers et al. (2014) use the integrated flux densities from Table A1 to calculate the luminosities for 38 of the MMB sources in the 20°–60° longitude range.

3.1 Remarks on sites of maser emission

In this section, we draw attention to specific sources which are not able to be fully described in Table 1 and Fig. 1. In particular, we highlight complex clusters of methanol masers, sources with interesting histories, parallax measurements and associations with other maser species.

G 22.356+0.066. Many of the spectral features of this source show periodic variations in flux density on a 178 d time-scale (Szymczak, Wolak & Bartkiewicz 2015).

G 23.010−0.410. Brunthaler et al. (2009) measured the trigonometric parallax of this source, deriving a distance of $4.59^{+0.38}_{-0.33}$ kpc, placing it in the Crux–Scutum spiral arm.

G 23.440−0.182. This maser is located at a distance of $5.88^{+1.37}_{-0.93}$ kpc as measured in the trigonometric parallax observations of Brunthaler et al. (2009) and shows emission from several

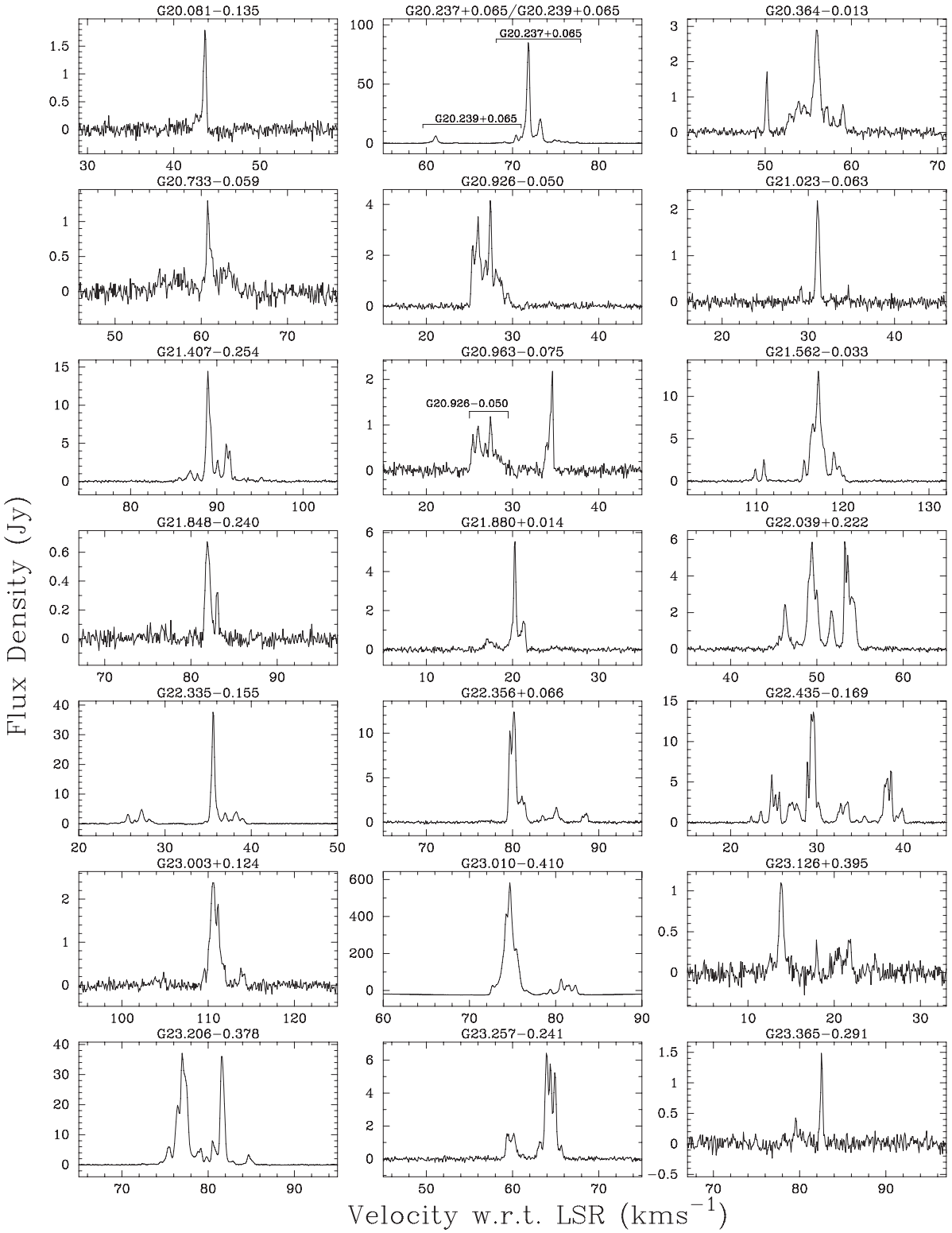

Figure 1. Spectra of 6668-MHz methanol masers. An asterisk (*) following the source name denotes spectra taken from the survey cube data and a double asterisk (**) denotes ATCA data.

class II methanol maser transitions, including the rare 37.7-GHz transition (Ellingsen et al. 2011, 2013).

G 23.657−0.127. Bartkiewicz et al. (2005) found that this maser shows a ring-like structure on VLBI-scales, suggesting that it may originate from a spherical bubble, or a face-on disc. Parallax observations (Bartkiewicz et al. 2008) of the accompanying 12.2-GHz methanol maser emission have placed this source at a distance of $3.19^{+0.46}_{-0.35}$ kpc. The spectral profile of this maser has remained remarkably stable and is unique, showing continuous emission from spectrally blended features over a velocity range of 11.9 km s^{-1}.

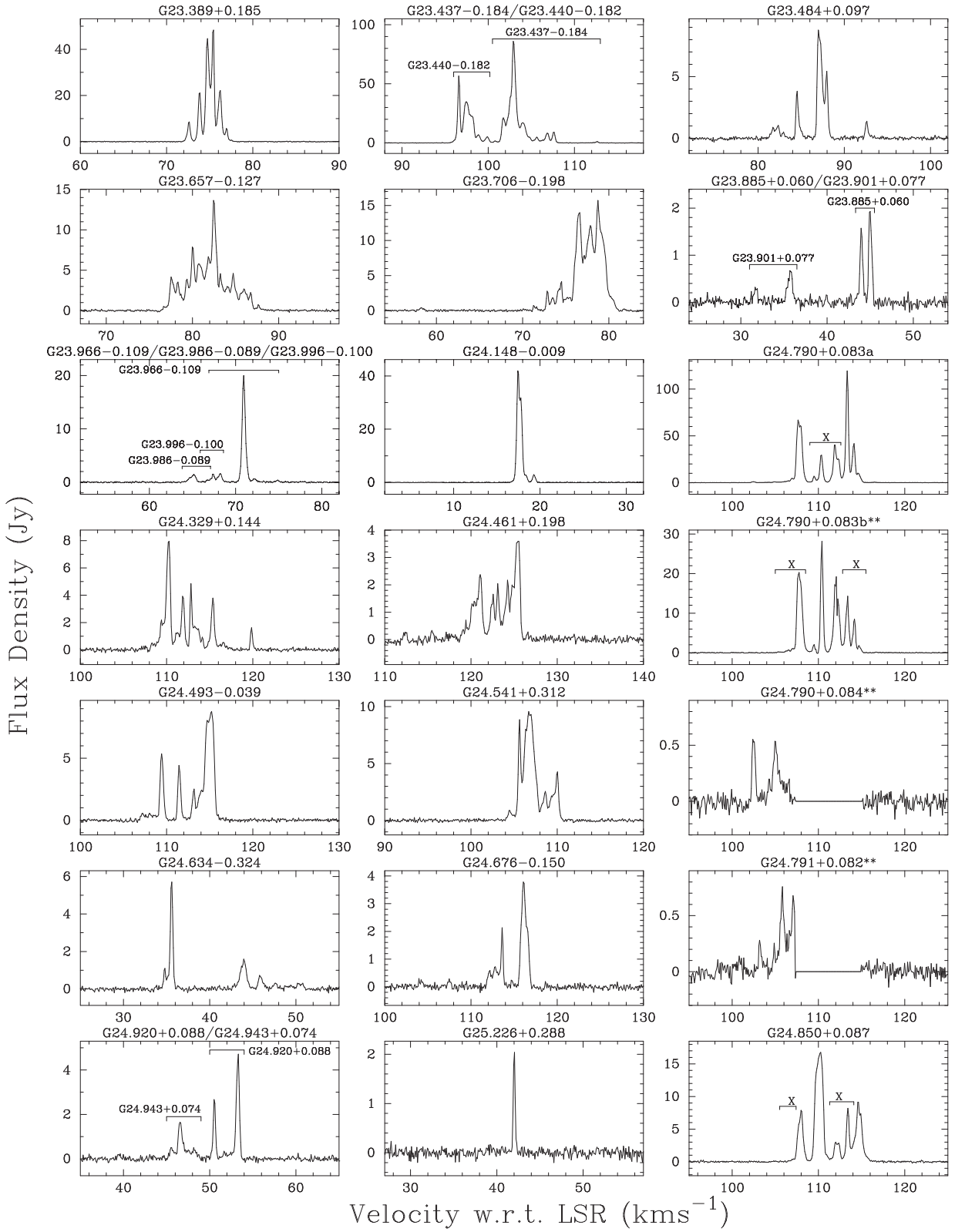

Figure 1 – *continued*

G 23.706−0.198. This source has a distance of $6.21^{+1.0}_{-0.80}$ kpc, measured through trigonometric parallax (Sanna et al. 2014).

G 24.790+0.083a, G 24.790+0.083b, G 24.790+0.084, G 24.791+0.082 and G 24.850+0.087. This cluster of masers consist of four sources that are located within 12 arcsec of each other, and then a further source that is located within 3 arcmin of the main cluster. In Fig. 1, we show ATCA spectra for G 24.790+0.083b, G 24.790+0.084 and G 24.791+0.082 where the additional spatial

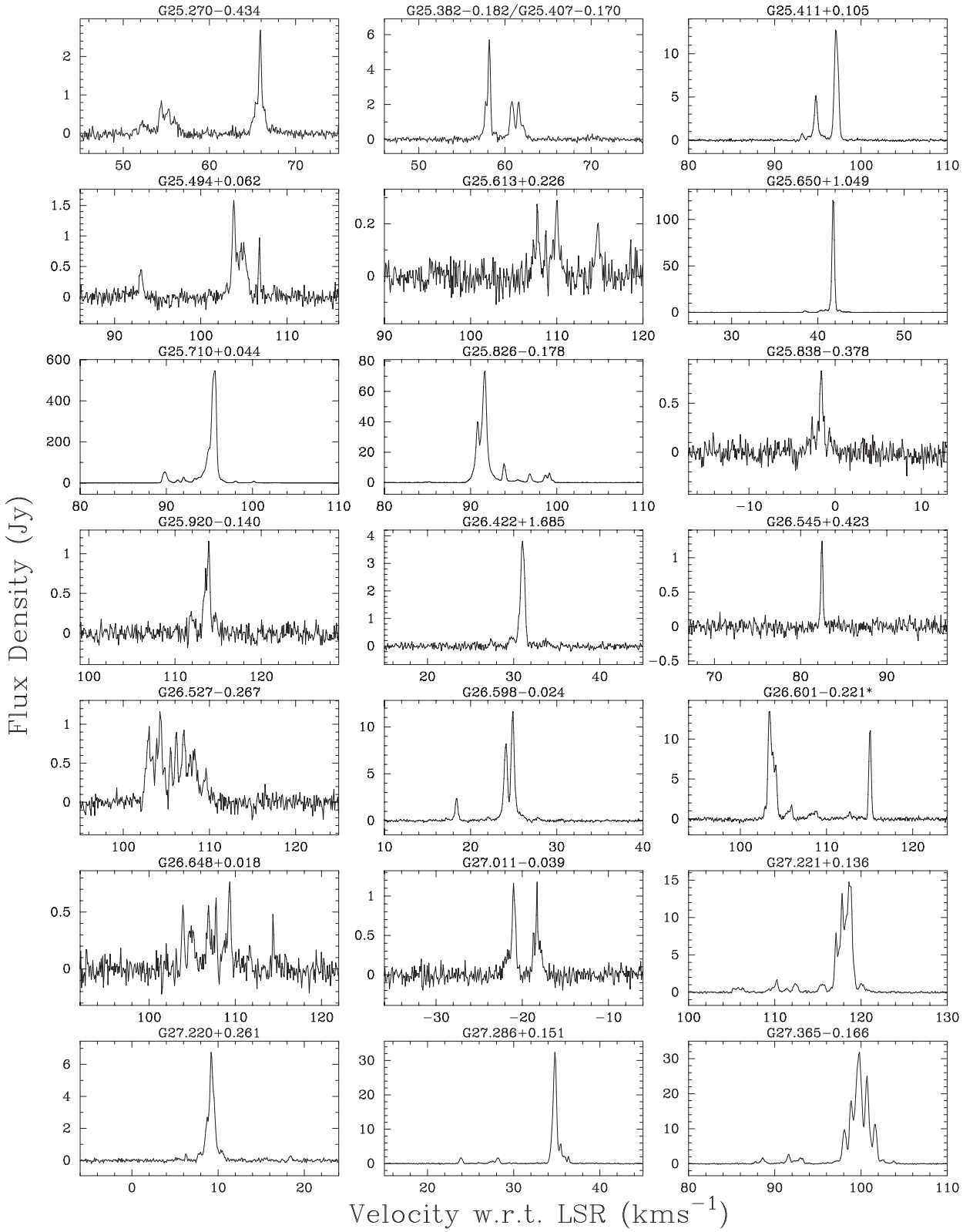

Figure 1 – *continued*

resolution allow them to be identified more easily. For the weaker sources (G 24.790+0.084 and G 24.791+0.082) we have zeroed the spectrum over the velocity range of strong artefacts from the nearby strong sources to allow their emission to be clearly seen. Owing to the complexity of the emission in this region, we have marked out the emission that is not located at each location with an 'X' as the confusing emission is often a combination from multiple nearby sources.

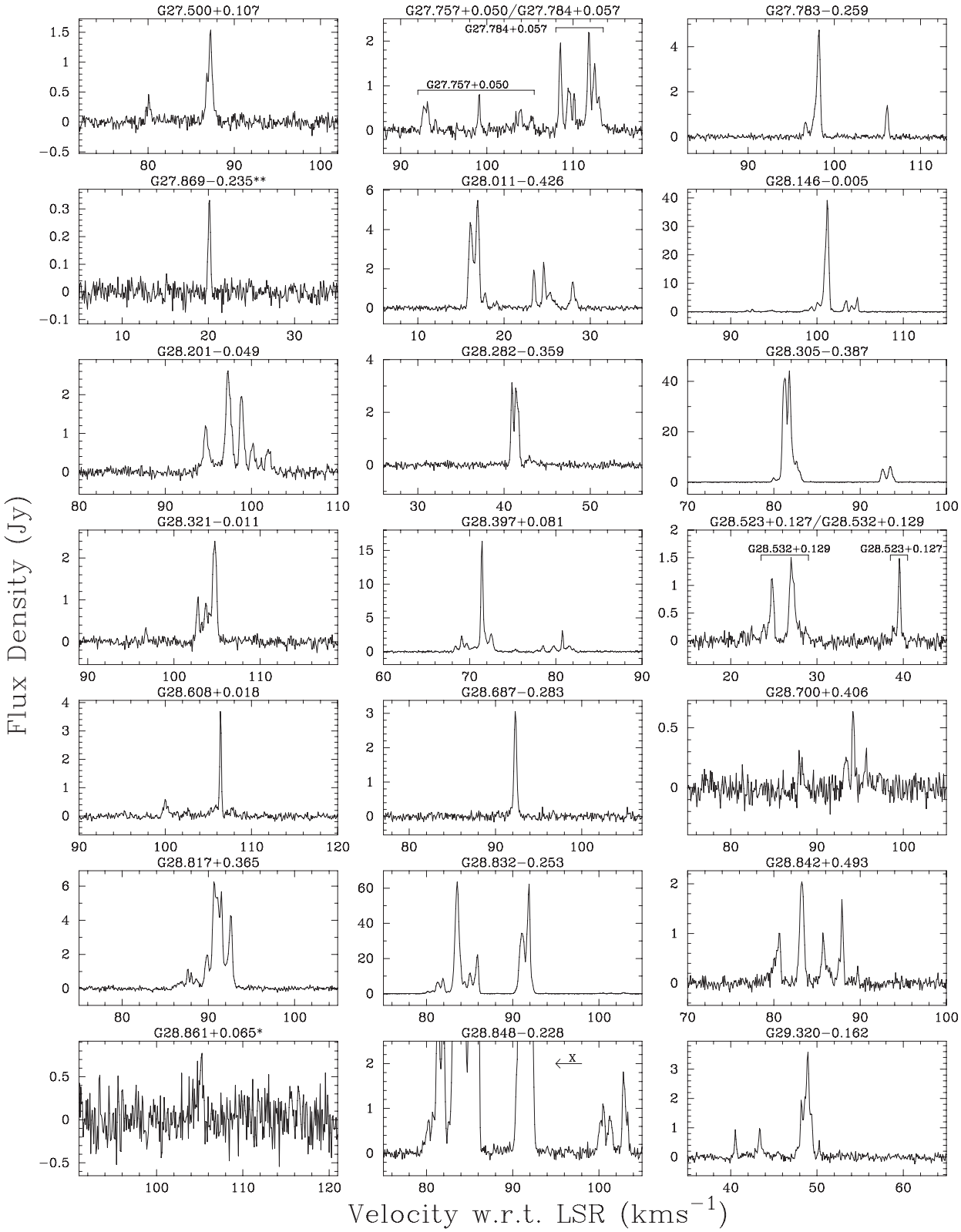

Figure 1 – *continued*

Two of these sources have been reported previously, G 24.790+0.083a (Walsh et al. 1998; Moscadelli et al. 2007) and G 24.790+0.083b (Moscadelli et al. 2007). Moscadelli et al. (2007) observed the methanol masers in this source with the EVN and our positions are in excellent agreement. We have used the ATCA positions in Table 1 for consistency with nearby sources. Moscadelli et al. (2007) present a thorough study of this star formation region, with observations of the 1665-MHz OH, 22-GHz water, 44- and

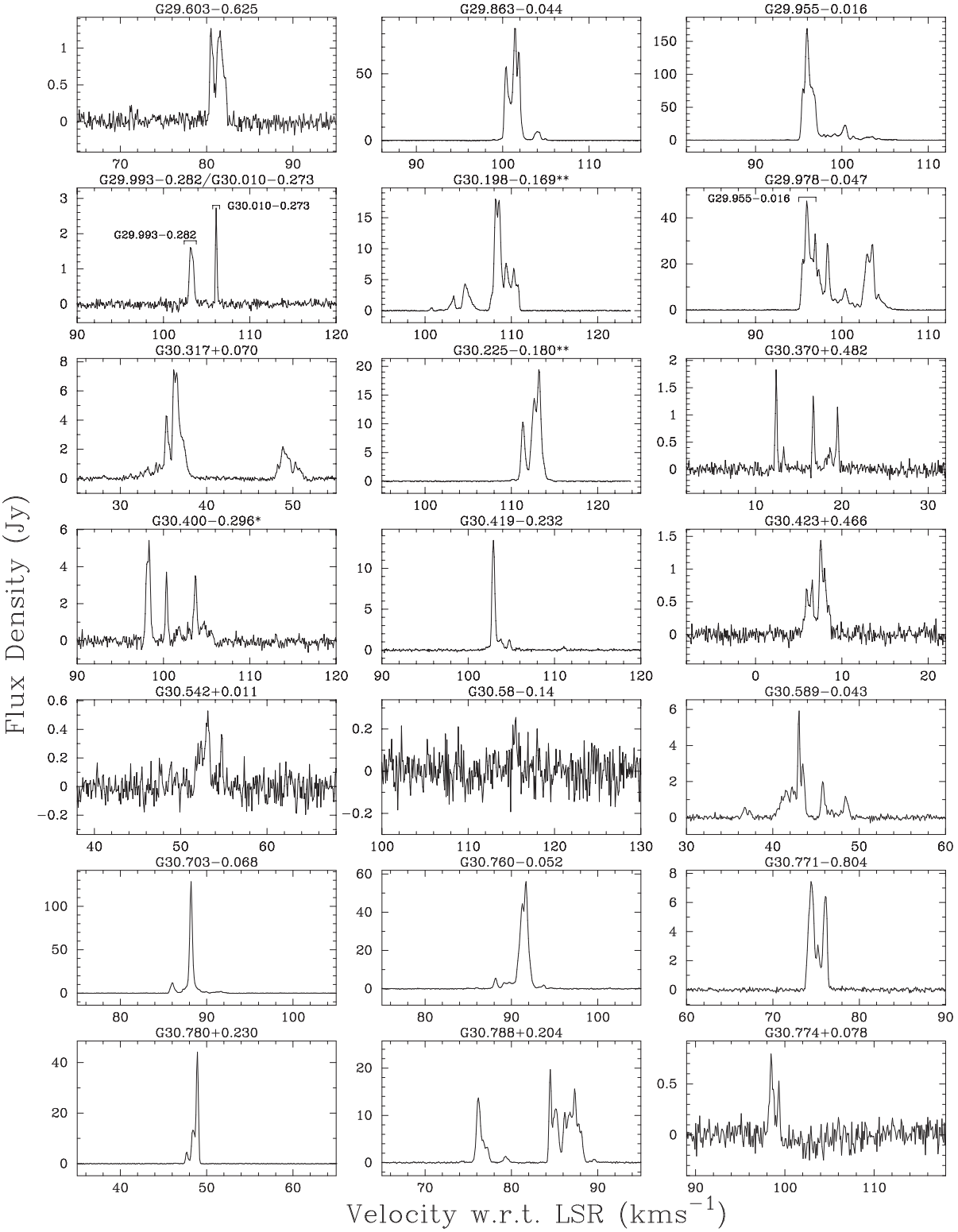

Figure 1 – *continued*

95-GHz class I methanol masers, a number of thermal lines and radio continuum emission.

G 25.411+0.105. Using monitoring data from the Torun telescope, Szymczak et al. (2015) found that this source exhibits periodic fluctuations in flux density. EVN observations of this maser have revealed a ring-like morphology of maser spots (Bartkiewicz et al. 2009).

G 27.365−0.166. Xu et al. (2011) measured the trigonometric parallax of this source, deriving a distance of $8.0^{+4.0}_{-2.0}$ kpc.

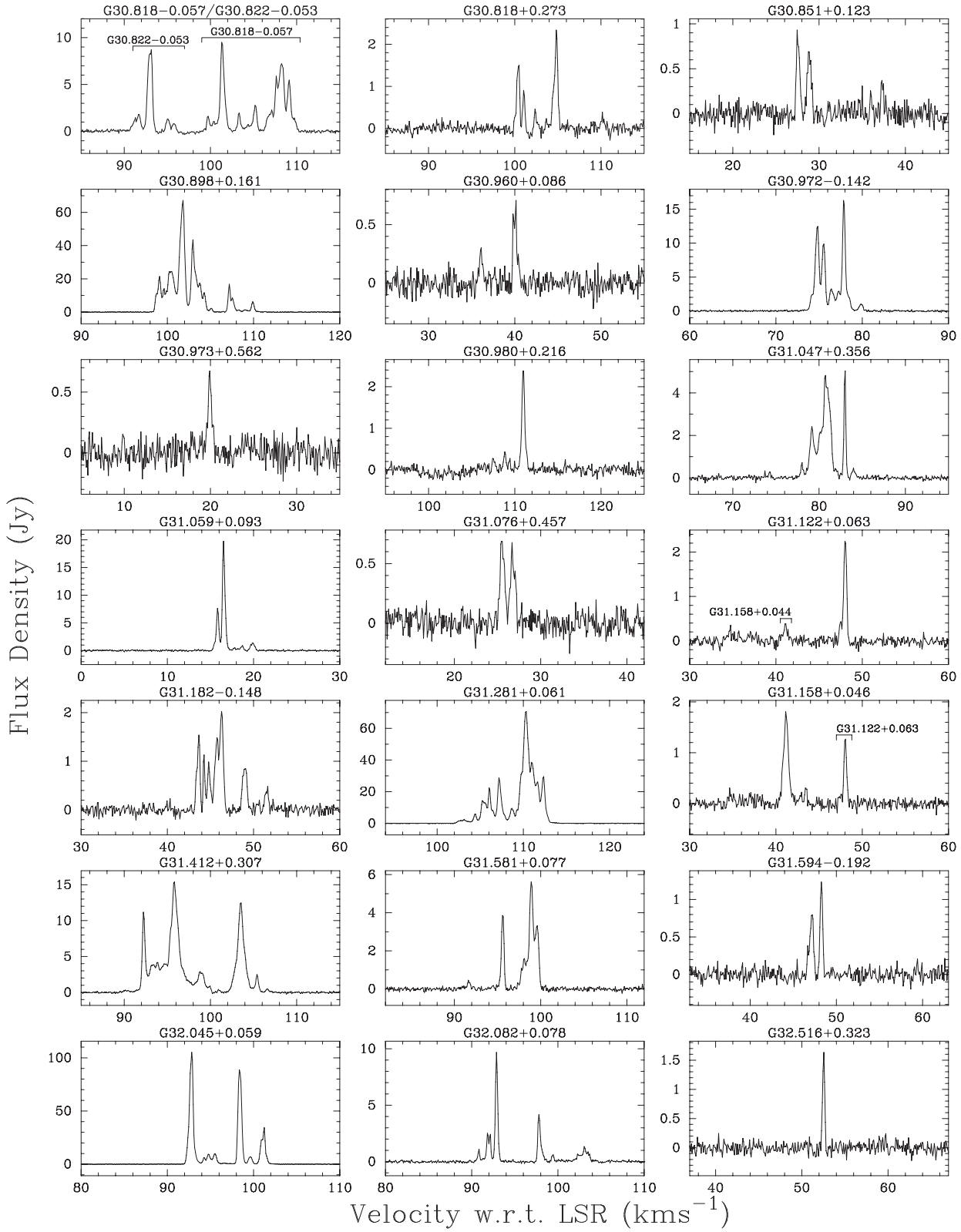

Figure 1 – *continued*

G 29.863−0.044, G 29.955−0.016, G 31.281+0.061 and G 31.581+0.077. These masers all fall within the W43 high-mass star-forming complex. Zhang et al. (2014) measured the trigonometric parallax for each of the sources (through observations of the 12-GHz methanol and water maser emission), finding an average distance of $5.49^{+0.39}_{-0.34}$ kpc.

G 31.412+0.307. This source has been studied in detail through numerous VLBI observations (Moscadelli et al. 2013), combining

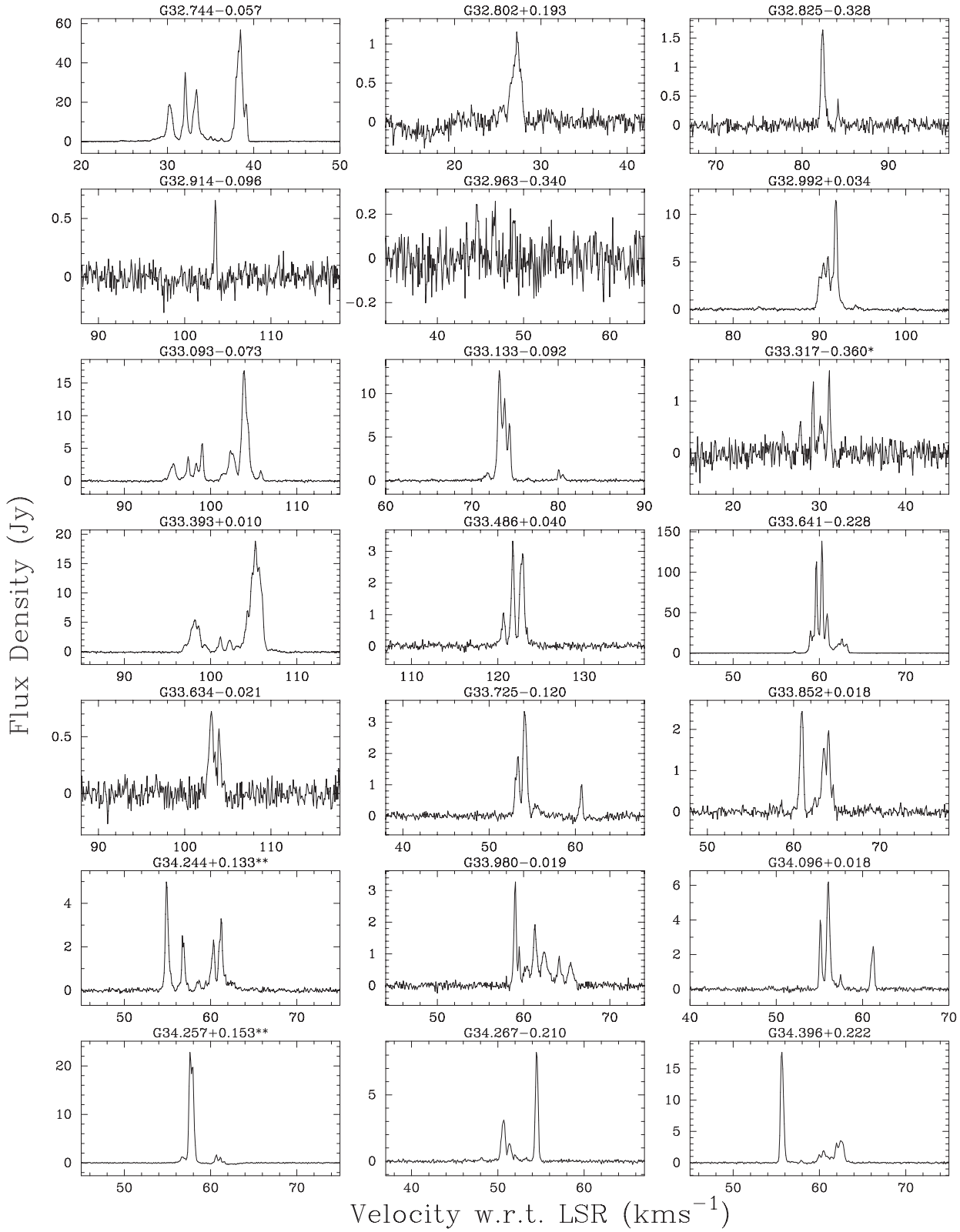

Figure 1 – *continued*

observations of the methanol maser emission with the accompanying emission of both water and OH masers. Moscadelli et al. (2013) report the detection of 85 methanol maser features, and were able to measure the proper motions of 40 of these, finding that they are mostly diverging from the centre of a hot molecular core, tracing the expansion driven by the double jet system.

G 30.58−0.14. This source was one of the weakest identified in the survey cubes at just 0.44 Jy. The follow-up MX revealed

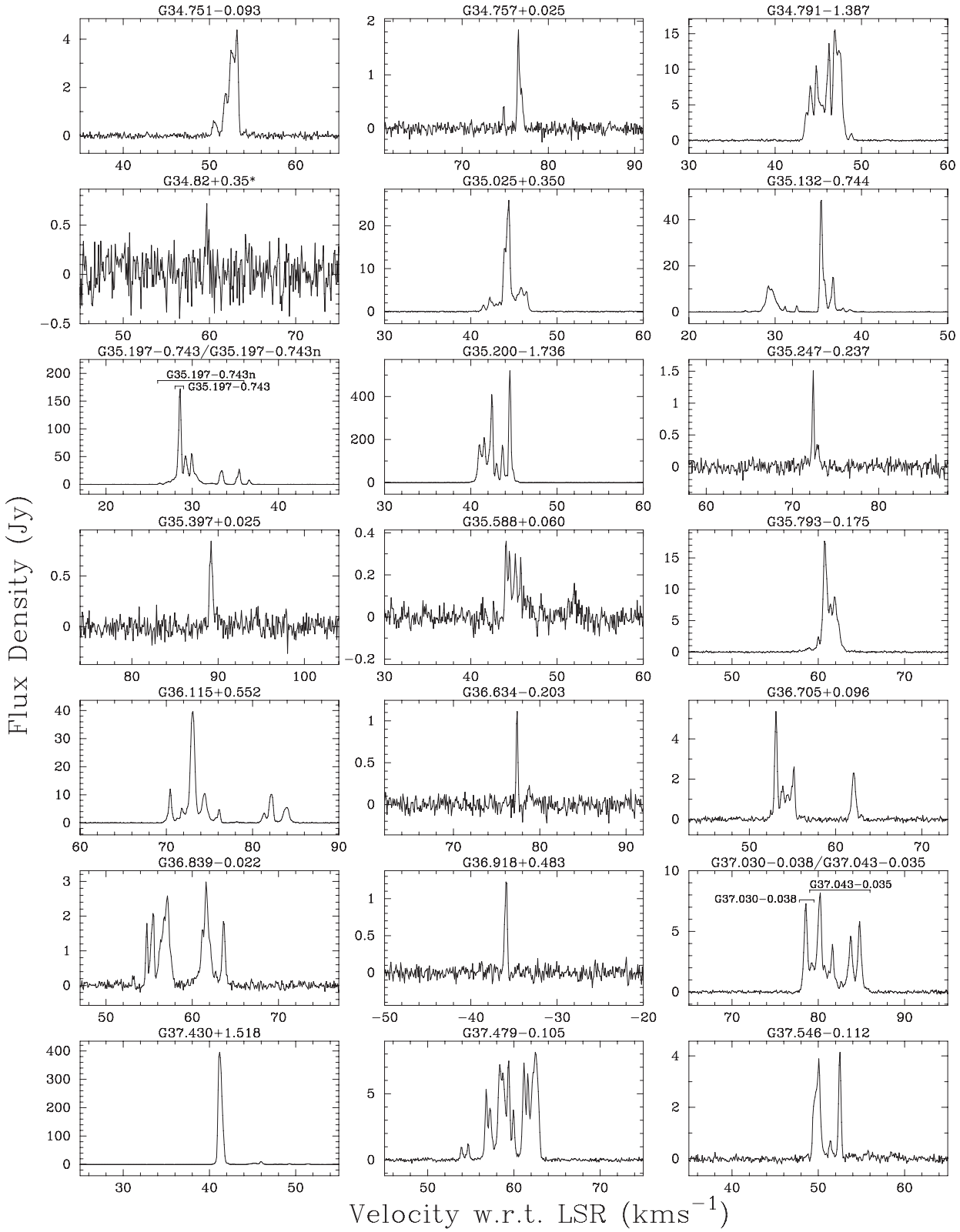

Figure 1 – *continued*

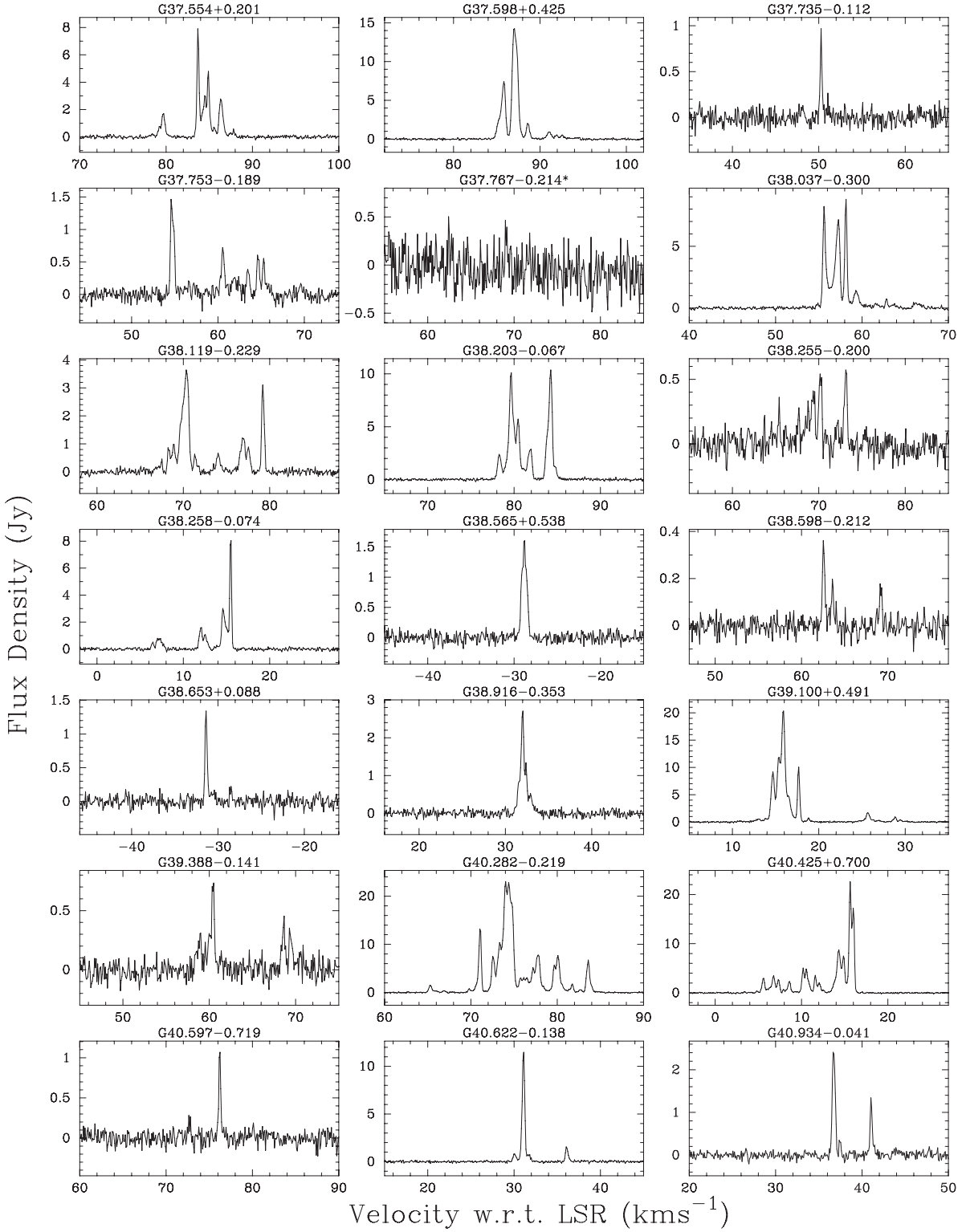

Figure 1 – *continued*

emission at the 0.3 Jy level and by the time we carried out our ATCA observations in 2014, the emission had fallen below our 5σ detection limit of 0.34 Jy.

G 32.045+0.059. Sato et al. (2014) measured the trigonometric parallax of this source, allowing them to derive a distance of $5.18^{+0.22}_{-0.21}$ kpc.

G 33.641−0.228. This maser has recently shown extreme bursting activity (Fujisawa et al. 2014b), with a total of five bursts detected between 2009 and 2012. Fujisawa et al. (2014b) found that burst occurred every 59 d on average and typically manifested itself as a large flux density rise (often more than a factor of 10) over about a day which then slowly

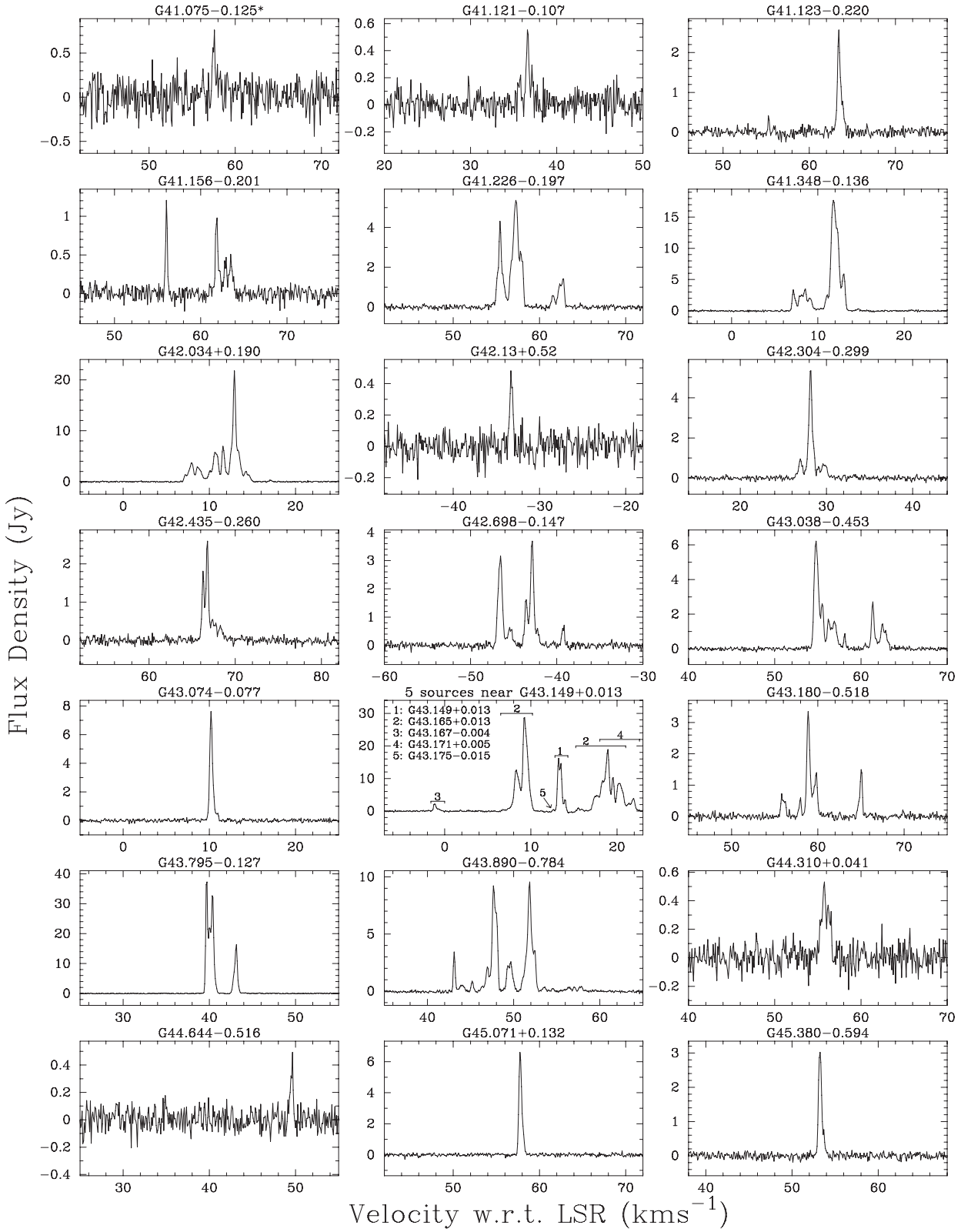

Figure 1 – *continued*

declined. This bursting activity occurred in a single spectral feature which the authors suggest is due to a rapid release of magnetic energy in the gas disc that surrounds the high-mass star.

The bursting feature has a velocity of $\sim$59.6 km s^{-1} which is the velocity of the peak emission detected in our MX observations, while in our survey cube observations the peak emission is at 60.3 km s^{-1} which is commonly seen as the peak spectral feature

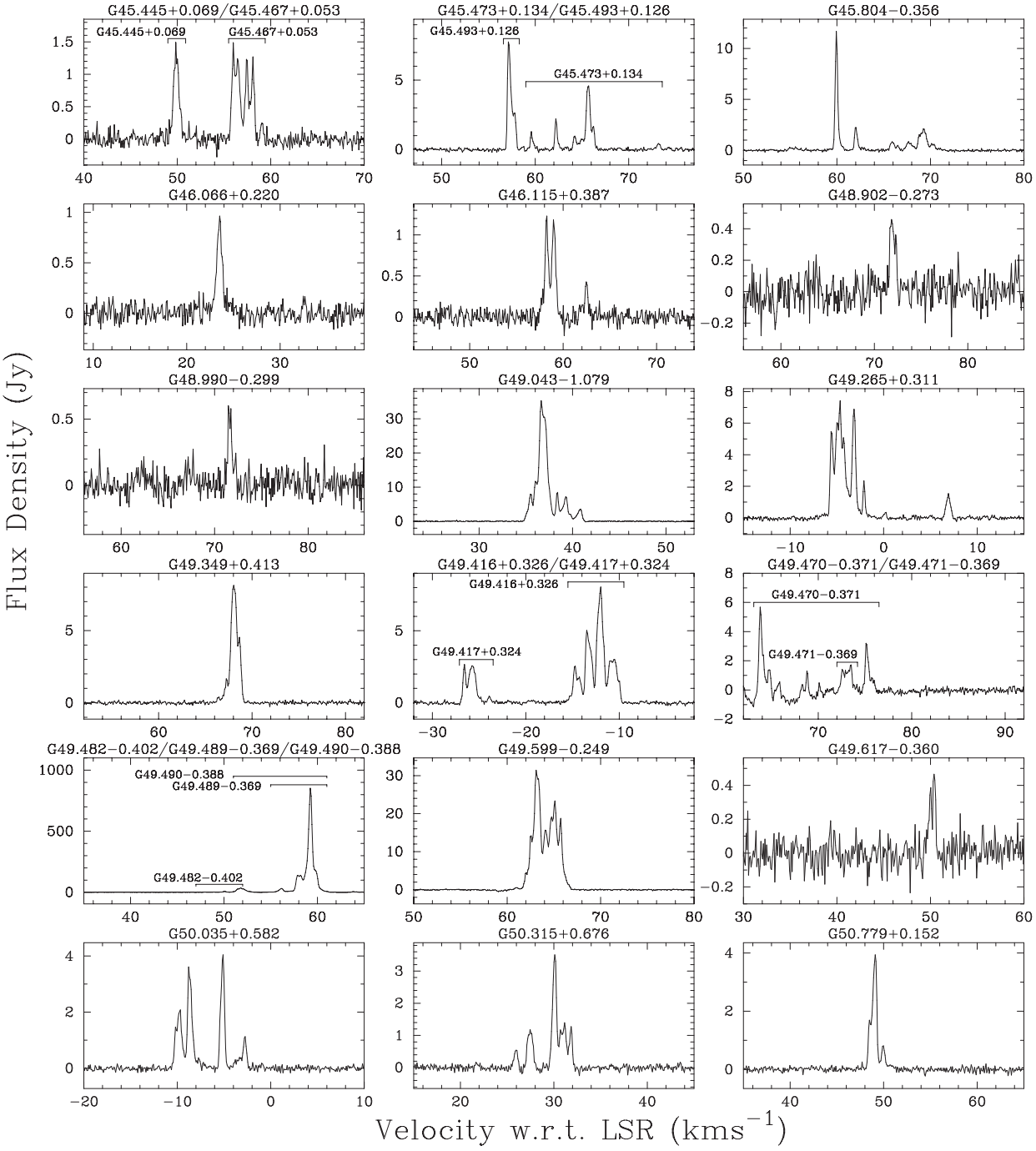

Figure 1 – *continued*

in the non-bursting state of this source. It is therefore likely that our MX observations occurred either during the rise or fall accompanying a bursting state, but since our MX observation (made on 2009 March 26) was made prior to the time when the Fujisawa et al. (2014b) observations began we cannot confirm this.

G 34.257+0.153. Slysh et al. (2001) conducted space-VLBI observations of both the 1665- and 1667-MH OH masers towards this source, allowing them to produce maser spot maps with an angular resolution of 1 mas.

G 34.396+0.222. Kurayama et al. (2011) derived a distance of $1.56^{+0.12}_{-0.11}$ kpc to this source through trigonometric parallax, showing that the kinematic distance was wrong by more than a factor of 2.

G 34.82+0.35. This maser was detected with a single spectral feature in the survey cube at 0.7 Jy, and then reduced to 0.2 Jy in the follow-up MX observation. By the time the ATCA observations were conducted in 2014, we were unable to detect any emission to a 5σ detection limit of 0.3 Jy. Pandian et al. (2007) also detected emission from this source in their Arecibo survey, with a peak of 0.24 Jy at the same velocity as we saw in our Parkes observations (59.7 km s^{-1}) and an additional weaker feature at a velocity of ∼58.5 km s^{-1}. Pandian et al. (2011) attempted to position this

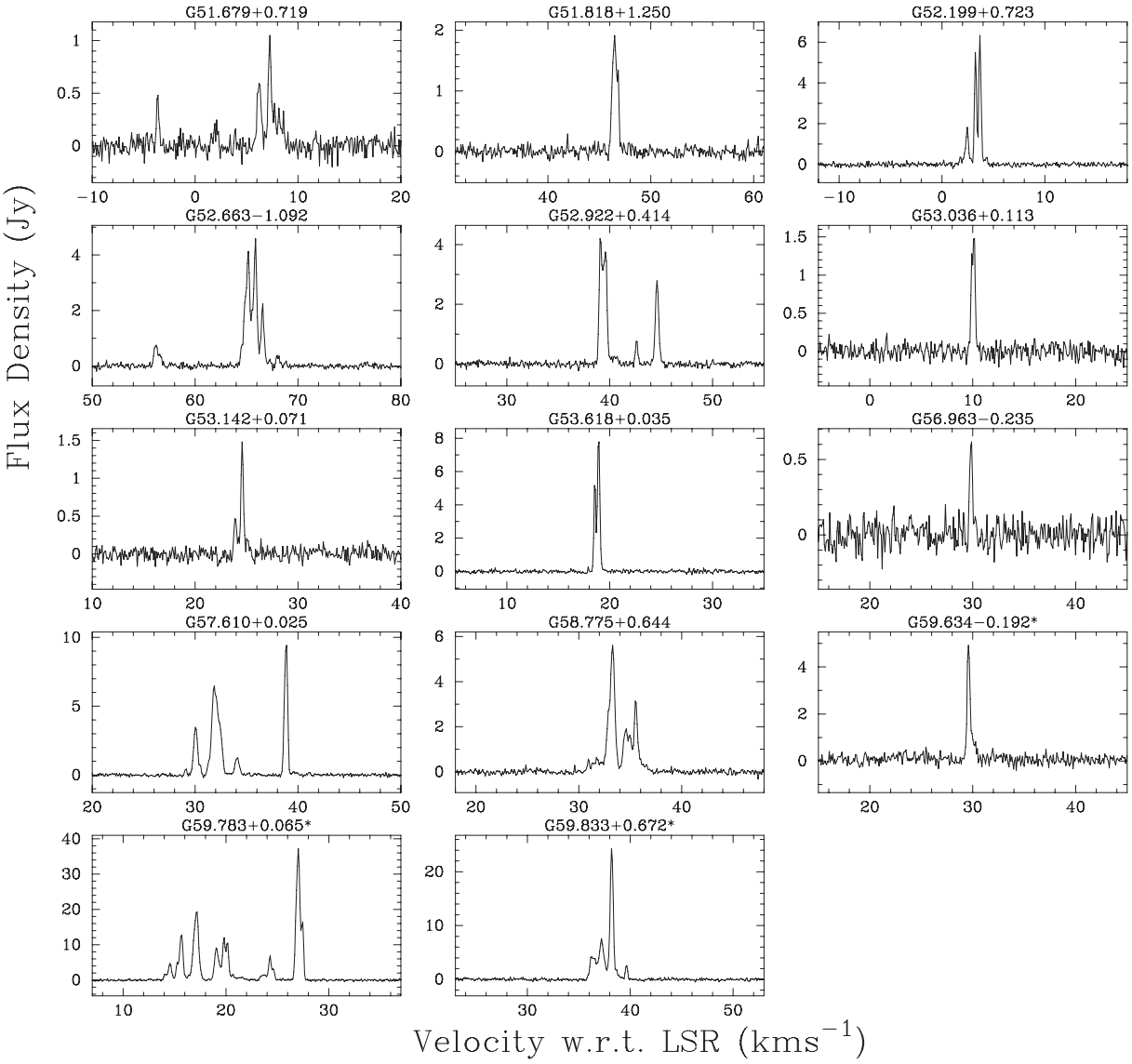

Figure 1 – *continued*

maser but failed, most likely due to variations in the peak flux density.

The position of this maser listed in Table 1 comes from our survey cube and is within 20 arcsec of the Pandian et al. (2007) single-dish position.

G 35.025+0.350. Wu et al. (2014) observed the trigonometric parallax of this source and determined a distance of $2.32^{+0.24}_{-0.20}$ kpc.

G 35.197−0.743 and G 35.197−0.743n. Our MERLIN observations show a close pair of sources, separated by just 2 arcsec. The slightly more southern source was observed in the VLBA observations of Zhang et al. (2009) resulting in a parallax distance of $2.19^{+0.24}_{-0.20}$ kpc. Surcis et al. (2012) detected high levels of linear polarization in several features (up to 11.5 per cent) indicative of a high level of saturation.

G 35.200−1.736. Located within the W48 complex, this source has a measured parallax distance of $3.27^{+0.56}_{-0.42}$ kpc (Zhang et al. 2009) placing it in the Carina–Sagittarius spiral arm. A detailed high-resolution polarization study (Surcis et al. 2012) revealed a high level of linear polarization in five spectral components (4.4–6.5 per cent).

This source shows a number of class II methanol maser transitions, including 12.2-GHz (e.g. Caswell et al. 1995), 107.0- and 156.6-GHz methanol masers (e.g. Caswell et al. 2000). This is also one of the first known 37.7-GHz methanol maser sources, originally detected as a 20 Jy source by Haschick, Baan & Menten (1989), falling to 3 Jy in 2005 observations with Onsala and then not detected in 2009, 2011 or 2012 in Mopra observations with a typical 3σ detection limit of 1 Jy (Ellingsen et al. 2011, 2013).

G 37.043−0.035. This source is located at a distance of $1.88^{+0.08}_{-0.08}$ kpc (Wu et al. 2014) as measured through trigonometric parallax observations.

G 37.546−0.112. Araya et al. (2010) monitored both the 6668-MHz methanol and 4829-MHz formaldehyde masers towards this source and found that it was the first example of a source with (quasi-)periodic correlated maser flares in both transitions.

G 42.13+0.52. This maser showed a single feature at $-33.4\,\mathrm{km\,s^{-1}}$ in the survey cube with a peak flux density of 0.86 Jy, falling to 0.5 Jy in the follow-up MX. In 2014, we attempted to position this maser with the ATCA but failed to detect any emission to a 5σ detection limit of 0.27 Jy. The position that we present in

Table 1 has been determined from our survey observations and we expect the true position of this source to be within 30 arcsec of the presented position.

G 43.149+0.013, G 43.165+0.013, G 43.167−0.004, G 43.171+0.005 and G 43.175−0.015. These five sources are all part of the W49 complex and are distributed over a couple of arcmininutes. All of the sources were detected Pandian et al. (2011) and with the exception of G 43.175−0.015 (which had a peak flux density as low as 0.5 Jy in our MX observation), were also detected by Caswell (2009).

G 43.165+0.013. Located within W49N, this source is located at a distance of $11.11^{+0.79}_{-0.69}$ (measured through observations of the nearby water maser Zhang et al. 2013), placing it in the Perseus arm.

G 43.795−0.127, G 43.890−0.784, G 45.071+0.132 and G 45.445+0.069. Wu et al. (2014) measured the trigonometric parallax of these four sources, deriving distances of $6.02^{+0.19}_{-0.18}$ kpc, $8.26^{+1.64}_{-1.17}$ kpc, $7.75^{+0.44}_{-0.40}$ kpc, $8.40^{+1.40}_{-1.05}$ kpc, respectively.

G 45.473+0.134. Szymczak et al. (2015) have recently shown that spectral feature at 59.6 km s^{-1} exhibits a periodicity of 195.7 d, finding that it has a stable flux density state of 1.3–1.4 Jy and a flare flux density of 3.6–8.6 Jy. In our observations, this spectral feature has a flux density of 1.3 Jy, indicating that the source was in the quiescent state at the time. Other spectral features associated with this source show weak flares which are synchronized with the main flaring feature.

G 49.470−0.371, G 49.471−0.369, G 49.482−0.402, G 49.489−0.369, G 49.490−0.388. These five sites all belong to the W51 complex. Caswell (2009) observed and positioned all five sources with the ATCA while Pandian et al. (2007) recognized only four sites in their Arecibo observations and consequently did not position G 49.471−0.369 in their follow-up observations (Pandian et al. 2011). In Table 1, we use the Pandian et al. (2011) positions where available as their MERLIN positions are probably slightly preferable, especially given the location of the sources in the Northern hemisphere. We do find an excellent correspondence with the Caswell (2009) positions which we have listed for G 49.471−0.369. We have used the Caswell (2009) velocity ranges to guide those values that we determine from our MX observations.

The masers in W51 have been investigated in some detail on VLBI scales, especially the 6668-MHz methanol and 6-GHz excited OH masers (Phillips & van Langevelde 2005; Etoka, Gray & Fuller 2012) and including 6668-MHz polarization studies at high resolution (Surcis et al. 2012).

G 49.489−0.369 has a trigonometric parallax distance of $5.1^{+2.9}_{-1.4}$ kpc (Xu et al. 2009b) and G 49.490−0.388 has a trigonometric parallax distance of $5.41^{+0.31}_{-0.28}$ kpc (Xu et al. 2009b; Sato et al. 2010).

4 DISCUSSION

This portion of the catalogue constitutes the final instalment of the MMB search for methanol masers in the section of the Galactic plane accessible from the Southern hemisphere. An analysis of the global properties of the full Galactic longitude range is being prepared (Green et al. in preparation) and is therefore beyond the scope of this paper. Here we limit our discussion to the sources within the specified longitude range and focus on the basic source statistics, distribution and variability. We also highlight a number of the MMB follow-up programmes, ongoing, completed and planned.

4.1 Basic source properties

Since the longitude range 20°–60° is accessible from the Northern hemisphere, where a number of previous searches have been carried out, there are fewer new detections in this range: 64 of the 265 sources that we detect. We find that the average peak flux density of the known sources is much higher at 31.6 Jy than the average peak flux density of the new sources at 5.9 Jy. This is the result of the combined effect of the often less sensitive surveys conducted previously and the tendency of *IRAS*-selected searches to be biased towards detecting the more luminous methanol masers. We further find that our new sources are located at slightly larger latitudes on average than the known sources (0.3 versus 0.2 deg), reflecting the fact that a large percentage of the low latitude sources have been detected in previous surveys (e.g. Pandian et al. 2007).

Of the newly discovered sources, the one with the highest flux density was G 32.045+0.059 which was discovered with a peak flux density of 163 Jy in the survey cube, and reduced to 105 Jy in the follow-up MX observation. The weakest new source we detected, G 30.58−0.14, was a mere 0.44 Jy in the initial survey, falling slightly to 0.3 Jy in the follow-up MX.

The detected masers range in flux density from 0.2 Jy to 965 Jy. The strongest maser that we detected in the survey observations was G 35.200−1.736 at 965.2 Jy (falling to 519.9 Jy in follow-up MX) and the weakest was G 27.869+0.235, identified at just 0.40 Jy. In the follow-up observations, G 49.490−0.388 shows the highest peak flux density (852.1 Jy), and G 34.82+0.35 the weakest at just 0.2 Jy.

As can be seen in Fig. 1, the masers we detect range in spectral profiles from single, narrow features to accumulations of many spectral components. The velocity ranges listed in Table 1 are given as the widest velocity spreads seen over all of the observations we have made. This means that our velocity ranges are not as susceptible to variability temporarily reducing the velocity ranges of the sources. The minimum velocity range for sources we detect is 0.3 km s^{-1}, representing those sources made up of a single spectral feature, and the largest is 23.7 km s^{-1}. The median velocity range is 7.0 km s^{-1} and there are 14 sources which have a velocity range of more than 16 km s^{-1}. Compared to other portions of the survey, this longitude range tends towards having slightly larger velocity ranges (for comparison, the median velocity range of sources in the 186°–330° longitude range is 5 km s^{-1}; Green et al. 2012a).

4.2 Source distribution

Within the 20°–60° longitude range we detect 265 6668-MHz methanol masers, equating to an average source density of 6.6 masers per degree of longitude, compared to the average density of the entire MMB survey region of 4.2. The density of sources in this section of the plane, however, is a lot less than the opposing 300°–340° longitude range, which has an average source density of 8.2 masers per degree of longitude, owing to the extremely high number of sources in the 330°–340° longitude range (which has more than 17 sources per degree of longitude).

Fig. 2 shows the longitude–latitude distribution of sources within the Galactic plane. Like other portions of the catalogue, we find there are few sources detected beyond latitudes of more than 1° from the plane. Within this longitude range, we find four sources at more extreme positive latitudes (G 25.650+1.049, G 26.422+1.685, G 37.430+1.518, G 51.818+1.250) and four at more negative latitudes (G 34.791−1.387, G 35.200−1.736, G 49.043−1.079,

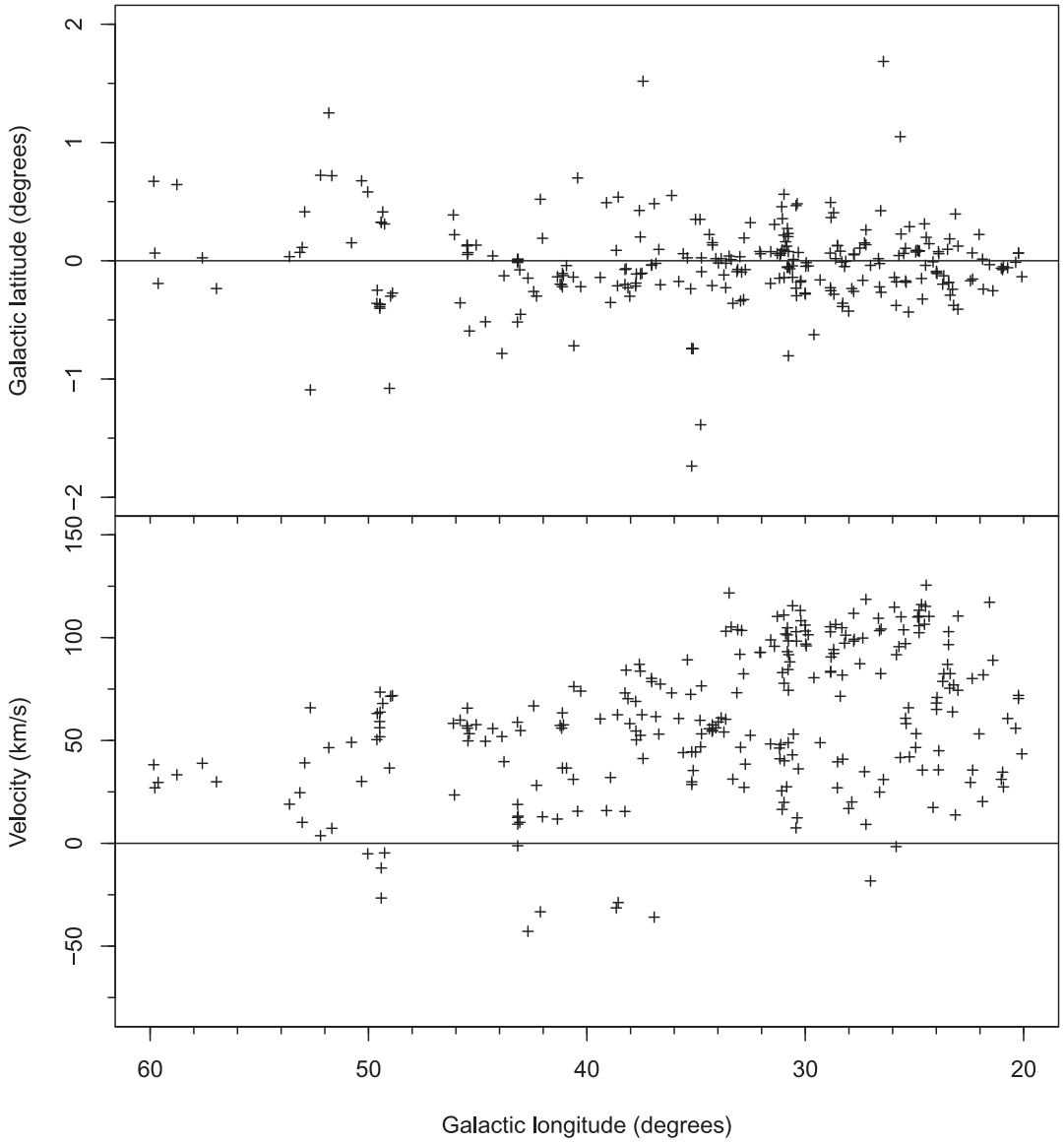

Figure 2. Distribution of the methanol masers in the Galactic longitude range 20°–60° (top) and distribution of the peak 6668-MHz methanol maser velocity versus Galactic longitude (bottom).

G 52.663−1.092). Also evident on the figure is the fall off in the density of sources detected between longitudes of ∼45° and 60°.

The bottom panel of Fig. 2 shows the velocity–longitude distribution of our detected methanol masers, highlighting the large range of allowed velocities in this region of the Galaxy and identifies those with negative velocities attributable to a far location outside the solar circle (with those around $-50\,\mathrm{km\,s^{-1}}$ most likely associated with the far side of the Crux–Scutum arm).

4.3 Variability

With few exceptions, masers detected in this longitude range were observed at least twice, allowing us to make a crude assessment of the level of temporal variability in these sources. Fig. 3 shows a comparison between the peak flux density measured in the initial survey observation versus the peak flux density measured in the follow-up observations. The follow-up observations plotted are chiefly MXs conducted with Parkes, but are supplemented with some ATCA values where MXs were not available. In the majority of instances, less than two years had passed between the survey observations and the presented follow-up observations, but in some cases as many as 7–8 years separate the observations.

The median ratio between the follow-up and survey peak flux density is 0.89, only slightly lower than that seen in the longitude ranges of the four other catalogue papers (0.92, 0.92, 0.98 and 0.99). The reason that these values are always less than 1 has been previously attributed to the greater effect of pointing offsets to the MXs than the survey cube data (which has been smoothed to a large effective beam size) and that the additional noise in the survey cube acts to increase the amplitude of weak sources that are several channels wide. In this particular longitude range, we sometimes targeted our MX observations towards source positions determined from the survey cubes (since the timing of observations meant that the final MX was conducted prior to the precise positions being

Table 2. Additional weak methanol masers from the literature within the 20°–60° longitude range not detected in the MMB survey. Sources names given to two decimal places have positions determined from single-dish observations. References are as follows: Olmi14: Olmi et al. (2014), Pan07: Pandian et al. (2007), Pan11: Pandian et al. (2011).

Source name	Equatorial coordinates		Velocity range				Refs
(l, b)	RA (2000)	Dec. (2000)	V_L	V_H	V_{pk}	S_{pk}	
(° °)	(h m s)	(° ′ ″)	(km s^{-1})		(km s^{-1})	(Jy)	
G 32.82−0.08	18 51 32.1	−00 07 51	58.4	60.3	–	0.05	Olmi14
G 33.09+0.06	18 51 30.5	+00 10 41	77.9	84.9	–	0.14	Olmi14
G 34.19−0.59	18 55 51.2	+00 51 18	57.6	63.1	–	0.22	Olmi14
G 34.71−0.59	18 56 48.2	+01 18 46	77.8	80.0	–	0.01	Olmi14
G 35.39+0.02	18 55 51.2	+02 11 37	94.0	97.2	96.9	0.19	Pan07
G 35.46+0.13	18 55 34.2	+02 19 11	73.2	74.4	–	0.02	Olmi14
G 35.57−0.03	18 56 22.6	+02 20 28	127.0	127.6	–	0.02	Olmi14
G 36.013−0.197	18 57 45.87	+02 39 05.7	92.4	93.5	93.0	0.16	Pan07, Pan11
G 36.42−0.16	18 58 23.2	+03 02 11	71.4	72.3	–	0.03	Olmi14
G 36.90−0.41	19 00 08.6	+03 20 35	83.1	85.1	84.7	0.45	Pan07
G 37.19−0.41	19 00 43.4	+03 36 24	29.4	30.1	–	0.07	Olmi14
G 37.34−0.06	18 59 43.1	+03 53 39	51.3	52.6	–	0.02	Olmi14
G 37.381−0.082	18 59 51.59	+03 55 18.0	67.5	70.9	70.6	0.19	Pan07, Pan11
G 37.86−0.60	19 02 36.0	+04 07 03	49.3	54.2	–	0.19	Olmi14
G 38.076−0.265	19 01 47.32	+04 27 20.9	66.7	67.8	67.5	0.59	Pan07, Pan11
G 38.555+0.163	19 01 08.35	+05 04 36.7	23.1	32.1	31.5	0.18	Pan07, Pan11
G 39.54−0.38	19 04 53.5	+05 41 59	47.4	49.4	47.8	0.20	Pan07
G 39.99−0.64	19 06 39.9	+05 59 13	71.5	72.1	–	0.02	Olmi14
G 41.05−0.24	19 07 12.4	+07 06 25	65.0	65.7	–	0.12	Olmi14
G 41.268+0.373	19 05 23.61	+07 35 05.3	19.4	20.6	20.3	0.26	Pan07, Pan11
G 41.577+0.042	19 07 09.18	+07 42 25.2	10.4	12.3	11.9	0.22	Pan07, Pan11
G 41.87−0.10	19 08 10.8	+07 54 04	15.5	23.7	15.8	0.22	Pan07
G 43.10+0.04	19 09 59.7	+09 03 58	8.8	10.1	–	0.02	Olmi14
G 43.53+0.01	19 10 52.9	+09 25 44	51.6	52.9	–	0.09	Olmi14
G 45.568−0.120	19 15 13.15	+11 10 16.5	1.2	9.8	1.6	0.40	Pan07, Pan11
G 46.32-0.25	19 17 09.0	+11 46 24	41.5	41.9	–	0.02	Olmi14
G 47.04+0.25	19 16 41.5	+12 39 19	101.5	102.0	–	0.02	Olmi14
G 48.89−0.17	19 21 47.5	+14 04 58	57.2	57.5	57.3	0.13	Pan07

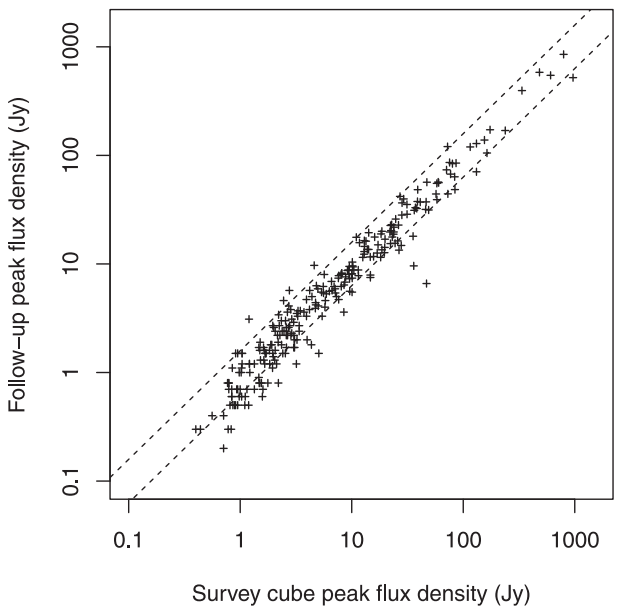

Figure 3. Comparison between the peak flux density of the initial survey cube spectrum versus the peak flux density measured in the follow-up observations (chiefly MXs carried out with Parkes). Sources that lie within the dashed lines have varied by less than a factor of 2.

determined), accounting for the small additional offset from a ratio of 1 compared to the other longitude regions.

We find that the peak flux density of three sources increased by more than a factor of 2 and that 15 sources decreased by more than a factor of 2. The high number of sources that have reduced by a factor of 2 or more is undoubtedly compounded by the tendency for a number of the follow-up observations to be conducted prior to obtaining a precise position. Otherwise, the overall level of variability is comparable to other portions of the survey.

4.4 Weak masers detected with Arecibo

Sensitive Arecibo searches conducted by Pandian et al. (2007) and Olmi et al. (2014) have detected a total of 28 methanol masers within our survey range in addition to the sources we detect. These masers are given in Table 2 and have peak flux densities ranging from 0.01 to 0.59 Jy, mostly falling well below the MMB detection limit.

Olmi et al. (2014) listed a number of further detections, but the MMB survey results have allowed us to determine that they are either far-side detections of strong masers located some tenths of degrees away (and sometimes even further), or spurious assignments of MMB detections located near their targets. In particular, we find that Olmi et al. (2014) sources G 33.13−0.09, G 34.37+0.23, G 35.13−0.74, G 36.83−0.02, G 37.04−0.03, G 56.96−0.23, G 59.63−0.19 correspond to the MMB sources G 33.133−0.092, G 34.396+0.222, G 34.132−0.744,

Table 3. Olmi et al. (2014) sources we believe are artefacts of nearby MMB sources (and have therefore omitted them from Table 2).

Olmi et al. (2014) source name (l, b) (° °)	Corresponding MMB source MMB source (l, b) (° °)
G 32.11+0.09	G 32.082+0.078
G 32.14+0.13	G 32.045+0.059
G 32.74−0.07	G 32.744−0.057
G 33.59−0.03	G 33.634−0.021
G 33.61−0.03	G 33.634−0.021
G 33.65−0.02	G 33.634−0.021
G 34.08+0.01	G 34.096+0.018
G 35.14−0.75	G 34.132−0.744
G 38.93−0.36	G 38.916−0.353
G 41.13−0.19	G 41.156−0.201
G 41.16−0.18	G 41.156−0.201
G 45.87−0.37	G 45.804−0.356
G 59.78+0.63	G 59.833+0.672

G 36.839−0.022, G 37.030−0.038, G 37.043−0.035 (previous two are blended in their single-dish observations), G 56.963−0.235 and G 59.634−0.191, respectively. We list a further 13 sources in Table 3 that we expect are artefacts of MMB sources, detected at various distances from the MMB location.

Given the much higher sensitivity of the Pandian et al. (2007) and Olmi et al. (2014) searches, the fact that there are only 28 additional sources is a strong indication that the MMB survey has missed very few of the methanol masers within our Galaxy due to sensitivity limitations (and is consistent with predictions presented in Pestalozzi et al. 2007). This is especially likely given the absence of any additional sources at negative velocities which would unambiguously place them at the far distance, outside the solar circle. When combined with our own more sensitive, targeted 'piggyback' survey (described in Green et al. 2009a) which is currently being prepared for publication, we will be able to not only assess the true completeness of the MMB survey, but also the luminosity distribution of the methanol maser population in our Galaxy.

4.5 MMB investigations and follow-up programmes

The MMB survey has produced a number of publications in addition to our main catalogue papers, presenting: our survey of the LMC and SMC (Green et al. 2008); the association between some of our masers with the 3-kpc arms (Green et al. 2009b); an investigation of the structure of our Galaxy (Green et al. 2011); the kinematic distance to many of the MMB sources using H I self-absorption to resolve ambiguities (Green & McClure-Griffiths 2011); and an investigation of the GLIMPSE counterparts to 776 of the MMB sources (Gallaway et al. 2013). There are also a number of further papers currently in preparation: the overall statistics of the entire MMB survey; our more sensitive 'piggyback' survey; and the Parkes excited OH survey that was conducted concurrently with the methanol observations.

Given the unbiased nature in which the MMB survey was conducted and the fact that each of the masers is unambiguously pinpointing elusive young high-mass stars (e.g. Minier et al. 2003; Breen et al. 2013), it has formed the target list for a number of follow-up observations. All of the MMB sources have been targeted for associated 12.2-GHz methanol maser emission, and the longitude range 186° through the Galactic Centre to 20° is published (Breen et al. 2012a, 2012b, 2014), as well as the overall statistics of the detections (Breen et al. 2011). The MMB sources are also being followed up for the four ground-state, main-line OH maser transitions in the MAGMO survey (Green et al. 2012b), and for 22-GHz water maser emission (Titmarsh et al. 2013, 2014). de Villiers et al. (2014) used the James Clerk Maxwell Telescope (JCMT) to observe a subset of the MMB masers, uncovering the characteristics of their associated CO outflow emission, explored in greater detail in de Villiers et al. (2015). Finally, investigations of the radio continuum emission and class I methanol maser counterparts are ongoing.

Together, this wealth of data promises to uncover further details about the methanol masers themselves and the high-mass star formation regions in which they reside.

5 SUMMARY

We present the final instalment of the MMB survey catalogue, covering the longitude range 20°–60°, completing the Southern hemisphere component of the survey. Within this longitude range we detect 265 6668-MHz methanol masers, bringing the total number of MMB detections in the longitude range 186° (through the Galactic Centre) to 60° to 972 sources. The properties of the masers we detect are similar to other portions of the survey; most of the detected masers are located within ±1° of the Galactic plane, they have comparable velocity ranges and show similar levels of variability. There are relatively fewer new methanol masers detected in this longitude range, reflecting the higher number of previous searches targeted towards this portion of the Galactic plane. Comparison with more sensitive, but smaller searches confirms that the MMB survey is not missing a large population of low flux density sources due to sensitivity limitations, which will be further explored with our own more sensitive 'piggyback' search in a future publication. We note a number of MMB follow-up programmes, focusing on transitions of OH, 12.2-GHz methanol and 22-GHz water masers, radio continuum and CO outflows, as well as comparisons with GLIMPSE sources, and, importantly, the upcoming overall statistics of the full MMB source list.

Digital versions of the spectra, together with various ancillary data, can be obtained at www.astromasers.org or www.manchester.ac.uk/joderallbank/mmb.

ACKNOWLEDGEMENTS

The Parkes telescope and the ATCA are both part of the Australia Telescope which is funded by the Commonwealth of Australia for operation as a National Facility managed by CSIRO. Financial support for this work was provided by the Australian Research Council. This research has made use of NASA's Astrophysics Data System Abstract Service; and the SIMBAD data base, operated at CDS, Strasbourg, France. SLB is the recipient of an Australian Research Council DECRA Fellowship (project number DE130101270). The authors dedicate this paper to the memory of J. L. Caswell, who was the driving force behind the MMB survey, and will continue to inspire maser studies for years to come.

REFERENCES

Araya E. D., Hofner P., Goss W. M., Kurtz S., Richards A. M. S., Linz H., Olmi L., Sewiło M., 2010, ApJ, 717, 133

Bartkiewicz A., Szymczak M., van Langevelde H. J., 2005, A&A, 442, L61

Bartkiewicz A., Brunthaler A., Szymczak M., van Langevelde H. J., Reid M. J., 2008, A&A, 490, 787
Bartkiewicz A., Szymczak M., van Langevelde H. J., Richards A. M. S., Pihlström Y. M., 2009, A&A, 502, 155
Bartkiewicz A., Szymczak M., van Langevelde H. J., 2014, A&A, 564, 110
Beuther H., Walsh A., Schilke P., Sridharan T. K., Menten K. M., Wyrowski F., 2002, A&A, 390, 289
Breen S. L., Ellingsen S. P., Caswell J. L., Lewis B. J., 2010, MNRAS, 401, 2219
Breen S. L., Ellingsen S. P., Caswell J. L., Green J. A., Voronkov M. A., Fuller G. A., Quinn L. J., Avison A., 2011, ApJ, 733, 80
Breen S. L., Ellingsen S. P., Caswell J. L., Green J. A., Voronkov M. A., Fuller G. A., Quinn L. J., Avison A., 2012a, MNRAS, 246, 2189
Breen S. L., Ellingsen S. P., Caswell J. L., Green J. A., Voronkov M. A., Fuller G. A., Quinn L. J., Avison A., 2012b, MNRAS, 421, 1703
Breen S. L., Ellingsen S. P., Contreras Y., Green J. A., Caswell J. L., Stevens J. B., Dawson J. R., Voronkov M. A., 2013, MNRAS, 435, 524
Breen S. L., Ellingsen S. P., Caswell J. L., Green J. A., Voronkov M. A., Fuller G. A., Quinn L. J., Avison A., 2014, MNRAS, 438, 3368
Brunthaler A., Reid M. J., Menten K. M., Zheng X. W., Moscadelli L., Xu Y., 2009, ApJ, 693, 424
Caswell J. L., 2009, PASA, 26, 454
Caswell J. L., Vaile R. A., Ellingsen S. P., Norris R. P., 1995, MNRAS, 274, 1126
Caswell J. L., Yi J., Booth R. S., Cragg D. M., 2000, MNRAS, 313, 599
Caswell J. L. et al., 2010, MNRAS, 404, 1029
Caswell J. L. et al., 2011, MNRAS, 417, 1964
Cragg D. M., Sobolev A. M., Godfrey P. D., 2005, MNRAS, 360, 533
Cyganowski C. J., Brogan C. L., Hunter T. R., Churchwell E., 2009, ApJ, 702, 1615
Dame T. M., Hartmann D., Thaddeus P., 2001, ApJ, 547, 792
de Villiers H. M. et al., 2014, MNRAS, 444, 566
de Villiers H. M. et al., 2015, MNRAS, 449, 119
Ellingsen S. P., 2007, MNRAS, 377, 571
Ellingsen S. P., Breen S. L., Sobolev A. M., Voronkov M. A., Caswell J. L., Lo N., 2011, ApJ, 742, 109
Ellingsen S. P., Breen S. L., Voronkov M. A., Dawson J. R., 2013, MNRAS, 429, 3501
Etoka S., Gray M. D., Fuller G. A., 2012, MNRAS, 423, 647
Fujisawa K. et al., 2014a, PASJ, 66, 31
Fujisawa K. et al., 2014b, PASJ, 66, 109
Gallaway M. et al., 2013, MNRAS, 430, 808
Green J. A., McClure-Griffiths N., 2011, MNRAS, 417, 2500
Green J. A. et al., 2008, MNRAS, 385, 948
Green J. A. et al., 2009a, MNRAS, 392, 783
Green J. A., McClure-Griffiths N. M., Caswell J. L., Ellingsen S. P., Fuller G. A., Quinn L., Voronkov M. A., 2009b, ApJ, 696, 156
Green J. A. et al., 2010, MNRAS, 409, 913
Green J. A. et al., 2011, ApJ, 733, 27
Green J. A. et al., 2012a, MNRAS, 420, 3108
Green J. A., McClure-Griffiths N. M., Caswell J. L., Robishaw T., Harvey-Smith L., 2012b, MNRAS, 425, 2530
Haschick A. D., Baan W. A., Menten K. M., 1989, ApJ, 346, 330
Kurayama T., Nakagawa A., Sawada-Satoh S., Sato K., Honma M., Sunada K., Hirota T., Imai H., 2011, PASJ, 63, 513
Minier V., Ellingsen S. P., Norris R. P., Booth R. S., 2003, A&A, 403, 1095
Moscadelli L., Goddi C., Cesaroni R., Beltran M. T., Furuya R. S., 2007, A&A, 472, 867
Moscadelli L., Sanna A., Goddi C., 2011, A&A, 536, 38
Moscadelli L., Li J. J., Cesaroni R., Sanna A., Xu Y., Zhang Q., 2013, A&A, 549, 122
Niezurawska A., Szymczak M., Richards A. M. S., Cohen R. J., 2005, Balt. Astron., 14, 429
Olmi L., Araya E. D., Hofner P., Molinari S., Morales Ortiz J., Moscadelli L., Pestalozzi M., 2014, A&A, 566, A18
Pandian J. D., Goldsmith P. F., Deshpande A. A., 2007, ApJ, 656, 255
Pandian J. D., Menten K. M., Goldsmith P. F., 2009, ApJ, 706, 1609
Pandian J. D., Momjian E., Xu Y., Menten K. M., Goldsmith P. F., 2011, ApJ, 730, 55
Pestalozzi M. R., Humphreys E. M. L., Booth R. S., 2002, A&A, 384, 15
Pestalozzi M. R., Chrysostomou A., Collett J. L., Minier V., Conway J., Booth R. S., 2007, A&A, 463, 1009
Phillips C. J., van Langevelde H. J., 2005, A&SS, 295, 225
Reid M. J. et al., 2014, ApJ, 783, 130
Sanna A. et al., 2014, ApJ, 781, 108
Sato M., Reid M. J., Brunthaler A., Menten K. M., 2010, ApJ, 720, 1055
Sato M. et al., 2014, ApJ, 793, 72
Slysh V. I. et al., 2001, MNRAS, 320, 217
Surcis G., Vlemmings W. H. T., van Langevelde H. J., Hutawarakorn Kramer B., 2012, A&A, 541, 47
Szymczak M., Hrynek G., Kus A. J., 2000, A&AS, 143, 269
Szymczak M., Kus A. J., Hrynek G., Kěpa A., Pazderski E., 2002, A&A, 392, 277
Szymczak M., Bartkiewicz A., Richards A. M. S., 2007, A&A, 468, 617
Szymczak M., Wolak P., Bartkiewicz A., Borkowski K. M., 2012, Astron. Nachr., 333, 634
Szymczak M., Wolak P., Bartkiewicz A., 2015, MNRAS, 448, 2284
Titmarsh A. M., Ellingsen S. P., Breen S. L., Caswell J. L., Voronkov M. A., 2013, ApJ, 775, 12
Titmarsh A. M., Ellingsen S. P., Breen S. L., Caswell J. L., Voronkov M. A., 2014, MNRAS, 443, 2923
Walsh A. J., Burton M. G., Hyland A. R., Robinson G., 1998, MNRAS, 301, 640
Wu Y. W. et al., 2014, A&A, 566, 17
Xu Y., Li J. J., Hachisuka K., Pandian J. D., Menten K. M., Henkel C., 2008, A&A, 485, 729
Xu Y., Voronkov M. A., Pandian J. D., Li J. J., Sobolev A. M., Brunthaler A., Ritter B., Menten K. M., 2009a, A&A, 507, 1117
Xu Y., Reid M. J., Menten K. M., Brunthaler A., Zheng X. W., Moscadelli L., 2009b, ApJ, 693, 413
Xu Y., Moscadelli L., Reid M. J., Menten K. M., Zhang B., Zheng X. W., Brunthaler A., 2011, ApJ, 733, 25
Zhang B., Zheng X. W., Reid M. J., Menten K. M., Xu Y., Moscadelli L., Brunthaler A., 2009, ApJ, 693, 419
Zhang B., Reid M. J., Menten K. M., Zheng X. W., Brunthaler A., Dame T. M., Xu Y., 2013, ApJ, 775, 79
Zhang B. et al., 2014, ApJ, 781, 89

APPENDIX A: 6668-MHZ INTEGRATED FLUX DENSITIES

Table A1 gives the integrated flux densities for sources across the full MMB survey range. The values for sources lying in the previously presented longitude ranges have been published as part of the 12.2-GHz methanol maser follow-up work Breen et al. (2012a,b, 2014). As stated in the 12.2-GHz catalogues, the data used to compute the 6668-MHz integrated flux densities is sometimes from a slightly different epoch than the spectra presented in the MMB catalogues and those data used to compute the tabulated properties.

Table A1. Integrated flux densities of the MMB sources. Columns 1, 3, 5 and 7 give the MMB source name, followed in each case by the integrated flux density (Jy km s^{-1}) of the 6668-MHz methanol maser emission. The presence of 'conf' in any of the even numbered columns indicates that the spectrum was confused with emission from nearby sources which prevented the integrated flux density from being determined. No value could be listed for G 208.996−19.386 because this source fell below the detection limit of all our MMB observations. Values derived from the survey cubes (rather than MX data) are marked with [sc] following the source name.

Source name	$I_{6.7}$	Source name	$I_{6.7}$	Source name	$I_{6.7}$	Source name	$I_{6.7}$
G 188.794+1.031	4.3	G 303.507−0.721	1.2	G 316.359−0.362	77	G 327.863+0.098	0.9
G 188.946+0.886	444	G 303.846−0.363	8.6	G 316.381−0.379	34	G 327.945−0.115	3.6
G 189.030+0.783	8.2	G 303.869+0.194	0.6	G 316.412−0.308	10	G 328.140−0.432	20
G 189.471−1.216	0.4	G 304.367−0.336	0.5	G 316.484−0.310	0.3	G 328.164+0.587	0.5
G 189.778+0.345	2.5	G 304.887+0.635	0.3	G 316.640−0.087	178	G 328.237−0.547	808
G 192.600−0.048	64	G 305.199+0.005	7.8	G 316.811−0.057	54	G 328.254−0.532	236
G 196.454−1.677	16	G 305.200+0.019	45	G 317.029+0.361	0.5	G 328.385+0.131	0.6
G 206.542−16.355	0.4	G 305.202+0.208	41	G 317.061+0.256	0.2	G 328.808+0.633	conf
G 208.996−19.386	–	G 305.208+0.206	375	G 317.466−0.402	93	G 328.809+0.633	conf
G 209.016−19.398	0.6	G 305.248+0.245	7.3	G 317.701+0.110	26	G 328.819+1.704	1.4
G 212.06−0.74	0.6	G 305.362+0.150	3.5	G 318.043−1.404	3.0	G 328.940+0.558	0.9
G 213.705−12.597	171	G 305.366+0.184	3.0	G 318.050+0.087	5.5	G 328.942+0.565	1.9
G 232.620+0.996	87	G 305.475−0.096	5.6	G 318.472−0.214	0.8	G 329.029−0.205	210
G 254.880+0.451	0.5	G 305.563+0.013	6.7	G 318.948−0.196	526	G 329.031−0.198	36
G 259.939−0.041	0.3	G 305.573−0.342	0.7	G 319.163−0.421	7.1	G 329.066−0.308	18
G 263.250+0.514	60	G 305.615−0.344	7.2	G 319.836−0.197	0.1	G 329.183−0.314	8.7
G 264.140+2.018	2.2	G 305.634+1.645	4.8	G 320.123−0.504	2.8	G 329.272+0.115	0.3
G 264.289+1.469	0.2	G 305.646+1.589	4.0	G 320.231−0.284	67	G 329.339+0.148	13
G 269.153−1.128	1.9	G 305.799−0.245	0.5	G 320.244−0.562	1.2	G 329.341−0.644	1.0
G 269.456−1.467	2.2	G 305.822−0.115	1.9	G 320.285−0.308	0.5	G 329.405−0.459	conf
G 269.658−1.270	3.1	G 305.887+0.017	4.5	G 320.414+0.109	1.2	G 329.407−0.459	conf
G 270.255+0.835	0.3	G 305.940−0.164	0.3	G 320.424+0.089	2.4	G 329.469+0.503	25
G 281.710−1.104	0.1	G 306.322−0.334	0.4	G 320.625+0.098	0.3	G 329.526+0.216	0.7
G 284.352−0.419	1.1	G 307.132−0.476	0.6	G 320.780+0.248	49	G 329.556+0.181	1.8
G 284.694−0.361	1.8	G 307.133−0.477	2.8	G 321.030−0.485	conf	G 329.610+0.114	32
G 285.337−0.002	11	G 308.056−0.396	0.5	G 321.033−0.483	conf	G 329.622+0.138	1.0
G 286.383−1.834	7.7	G 308.075−0.411	0.3	G 321.148−0.529	4.6	G 329.719+1.164	9.4
G 287.371+0.644	69	G 308.651−0.507	4.4	G 321.704+1.168	0.8	G 330.070+1.064	8.8
G 290.374+1.661	1.1	G 308.686+0.530	1.4	G 322.158+0.636	628	G 330.226+0.290	1.5
G 290.411−2.915	2.2	G 308.715−0.216	1.5	G 322.705−0.331	1	G 330.283+0.493	5.2
G 291.270−0.719	2.5	G 308.754+0.549	19	G 323.459−0.079	12	G 330.875−0.383	0.1
G 291.274−0.709	89	G 308.918+0.123	44	G 323.740−0.263	5121	G 330.878−0.367	0.4
G 291.579−0.431	1.2	G 309.384−0.135	0.6	G 323.766−1.370	0.9	G 330.953−0.182	4.4
G 291.582−0.435	1.7	G 309.901+0.231	17	G 323.793−0.397	0.8	G 330.998+0.093	0.4
G 291.642−0.546	0.1	G 309.921+0.479	1038	G 323.799+0.017	3.1	G 331.059+0.375	4.1
G 291.879−0.810	0.7	G 310.144+0.760	99	G 324.716+0.342	4.6	G 331.120−0.118	2.2
G 292.074−1.131	0.2	G 310.180−0.122	0.7	G 324.789−0.378	0.4	G 331.132−0.244	29
G 292.468+0.168	4.5	G 311.230−0.032	1.9	G 324.915+0.158	25	G 331.134+0.156	1.1
G 293.723−1.742	0.2	G 311.551−0.055	0.4	G 324.923−0.568	2.2	G 331.278−0.188	221
G 293.827−0.746	2.9	G 311.628+0.266	5.0	G 325.659−0.022	0.2	G 331.342−0.346	127
G 293.942−0.874	1.3	G 311.643−0.380	8.8	G 326.323−0.393	2.7	G 331.425+0.264	16
G 294.337−1.706	0.1	G 311.729−0.735	0.3	G 326.448−0.748	12	G 331.437−0.304	5.7
G 294.511−1.621	15	G 311.947+0.142	0.1	G 326.475+0.703	135	G 331.442−0.187	135
G 294.977−1.734[sc]	1.1	G 312.071+0.082	76	G 326.476+0.695	1.3	G 331.542−0.066	3.5
G 294.990−1.719	4.3	G 312.108+0.262	16	G 326.608+0.799	0.5	G 331.543−0.066	14
G 296.893−1.305	1.4	G 312.307+0.661	1.5	G 326.641+0.611	25	G 331.556−0.121	64
G 297.406−0.622	0.5	G 312.501−0.084	0.5	G 326.662+0.520	21	G 331.710+0.603	17
G 298.177−0.795	3.3	G 312.597+0.045	0.4	G 326.859−0.677	12	G 331.900−1.186	2.9
G 298.213−0.343	2.3	G 312.598+0.045	8.3	G 326.986−0.031	1.4	G 332.094−0.421	14
G 298.262+0.739	9.3	G 312.698+0.126	1.1	G 327.120+0.511	48	G 332.295−0.094	13
G 298.632−0.362	1.0	G 312.702−0.087	0.9	G 327.282−0.469	4.5	G 332.296−0.094	1.7
G 298.723−0.086	0.5	G 313.469+0.190	36	G 327.291−0.578	2.4	G 332.295+2.280	117
G 299.013+0.128	3.3	G 313.577+0.325	56	G 327.392+0.199	10	G 332.351−0.436	6.7
G 299.772−0.005	13	G 313.705−0.190	0.8	G 327.395+0.197	3.5	G 332.352−0.117	6.3
G 300.504−0.176	4.4	G 313.767−0.863	27	G 327.402+0.445	135	G 332.364+0.607	0.2
G 300.969+1.148	5.5	G 313.774−0.863	14	G 327.566−0.850	9.7	G 332.560−0.148	1.5
G 301.136−0.226	1.5	G 313.994−0.084	15	G 327.590−0.094	1.7	G 332.583+0.147	3.8
G 302.032−0.061	14	G 314.221+0.273	1.0	G 327.618−0.111	1.9	G 332.604−0.168	0.6
G 302.034+0.625	1.3	G 314.320+0.112	28	G 327.710−0.394	3.2	G 332.653−0.621	5.0
G 302.455−0.741	1.1	G 315.803−0.575	3.0	G 327.808−0.634	1.2	G 332.701−0.588	0.1

Table A1 *– continued*

Source name	$I_{6.7}$	Source name	$I_{6.7}$	Source name	$I_{6.7}$	Source name	$I_{6.7}$
G 332.726−0.621	7.3	G 336.881+0.008	2.1	G 339.294+0.139	7.6	G 345.824+0.044	1.7
G 332.813−0.701	7.3	G 336.916−0.024	2.4	G 339.476+0.185	5.7	G 345.949−0.268	0.6
G 332.826−0.549	3.3	G 336.941−0.156	48	G 339.477+0.043	2.5	G 345.985−0.020	4.4
G 332.854+0.817	0.6	G 336.957−0.225	2.9	G 339.582−0.127	11	G 346.036+0.048	8.5
G 332.942−0.686	9.1	G 336.958−0.977	0.5	G 339.622−0.121	141	G 346.231+0.119	1.6
G 332.960+0.135	1.4	G 336.983−0.183	16	G 339.681−1.208	69	G 346.480+0.221	22
G 332.963−0.679	28	G 336.994−0.027	20	G 339.682−1.207	conf	G 346.481+0.132	2.7
G 332.975+0.773	0.6	G 337.052−0.226	15	G 339.762+0.054	9.1	G 346.517+0.117	0.9
G 332.987−0.487	8.6	G 337.097−0.929	5.0	G 339.884−1.259	2568	G 346.522+0.085	0.6
G 333.029−0.015	7.5	G 337.132−0.068	1.8	G 339.909+0.240	0.3	G 347.230+0.016	0.3
G 333.029−0.063	0.8	G 337.153−0.395	15	G 339.949−0.539	195	G 347.583+0.213	6.3
G 333.068−0.447	9.3	G 337.176−0.032	7.0	G 339.980−0.538	2.1	G 347.628+0.149	6.9
G 333.109−0.500	0.6	G 337.201+0.114	23	G 339.986−0.425	109	G 347.631+0.211	5.4
G 333.121−0.434	19	G 337.202−0.094	3.6	G 340.034−1.110	3.4	G 347.817+0.018	4.3
G 333.126−0.440	4.0	G 337.258−0.101	17	G 340.054−0.244	39	G 347.863+0.019	8.7
G 333.128−0.440	1.3	G 337.263−0.070	0.9	G 340.118−0.021	0.8	G 347.902+0.052	6.4
G 333.135−0.431	0.4	G 337.300−0.874	4.3	G 340.182−0.047	3	G 348.027+0.106	4.5
G 333.128−0.560	14	G 337.388−0.210	43	G 340.249−0.046	19	G 348.195+0.768	1.9
G 333.130−0.560	15	G 337.404−0.402	76	G 340.249−0.372	0.2	G 348.550−0.979	81
G 333.163−0.101	5.4	G 337.517−0.348	0.3	G 340.518−0.152	6.4	G 348.550−0.979n	49
G 333.184−0.091	7.0	G 337.613−0.060	47	G 340.543−0.162	0.5	G 348.579−0.920	0.3
G 333.234−0.060	0.3	G 337.632−0.079	19	G 340.655−0.235	0.3	G 348.617−1.162	77
G 333.234−0.062	2.2	G 337.686+0.137	0.5	G 340.785−0.096	268	G 348.654+0.244	0.3
G 333.315+0.105	41	G 337.703−0.053	10	G 340.970−1.022	9.1	G 348.723−0.078	3.5
G 333.387+0.032	3.9	G 337.705−0.053	236	G 341.124−0.361	1.3	G 348.703−1.043	213
G 333.466−0.164	35	G 337.710+0.089	1.5	G 341.218−0.212	336	G 348.727−1.037	149
G 333.562−0.025	56	G 337.720+0.065	0.4	G 341.238−0.270	7.2	G 348.884+0.096	17
G 333.646+0.058	10	G 337.844−0.375	3.4	G 341.276+0.062	9.3	G 348.892−0.180	0.8
G 333.683−0.437	20	G 337.920−0.456	27	G 341.367+0.336	0.4	G 349.067−0.017	5.5
G 333.761−0.226	2.4	G 337.966−0.169	16	G 341.973+0.233	1.0	G 349.092+0.105	22
G 333.851+0.527	0.4	G 337.997+0.136	2.6	G 341.990−0.103	0.5	G 349.092+0.106	12
G 333.900−0.099	0.7	G 338.069+0.011	1.3	G 342.251+0.308	2.3	G 349.151+0.021	1.6
G 333.931−0.135	6.1	G 338.075+0.012	19	G 342.338+0.305	1.4	G 349.579−0.679	1.8
G 334.138−0.023	3.0	G 338.075+0.009	10	G 342.368+0.140	9.1	G 349.799+0.108	7.8
G 334.307−0.079	1.8	G 338.140+0.178	4.7	G 342.446−0.072	3.0	G 349.884+0.231	7.6
G 334.635−0.015	28	G 338.160−0.064	4.4	G 342.484+0.183	83	G 350.011−1.342	0.9
G 334.933−0.307	3.5	G 338.280+0.542	3.0	G 342.954−0.019	4.5	G 350.015+0.433	7.8
G 334.935−0.098	4.9	G 338.287+0.120	14	G 343.354−0.067	13	G 350.104+0.084	6.0
G 335.060−0.427	48	G 338.325−0.409	1.9	G 343.502−0.472	9.3	G 350.105+0.083	58
G 335.426−0.240	22	G 338.388+0.162	8.9	G 343.756−0.163	4.2	G 350.116+0.084	7.8
G 335.556−0.307	35	G 338.392−0.403	2.2	G 343.929+0.125	16	G 350.116+0.220	1.2
G 335.585−0.285	47	G 338.396−0.007	2.5	G 344.227−0.569	128	G 350.189+0.003	0.4
G 335.585−0.289	39	G 338.432+0.058	20	G 344.419+0.044	1.5	G 350.299+0.122	39
G 335.585−0.290	conf	G 338.461−0.245	145	G 344.421+0.045	11	G 350.340+0.141	1.2
G 335.726+0.191	39	G 338.472+0.289	0.7	G 344.581−0.024	2.8	G 350.344+0.116	21
G 335.789+0.174	378	G 338.497+0.207	2.2	G 345.003−0.223	227	G 350.356−0.068	1.2
G 335.824−0.177	0.2	G 338.561+0.218	87	G 345.003−0.224	120	G 350.470+0.029	1.1
G 336.018−0.827	181	G 338.566+0.110	2.0	G 345.010+1.792	513	G 350.520−0.350	0.9
G 336.358−0.137	21	G 338.850+0.409	1.4	G 345.012+1.797	53	G 350.686−0.491	11
G 336.409−0.257	5.3	G 338.875−0.084	13	G 345.131−0.174	2.1	G 350.776+0.138	0.5
G 336.433−0.262	42	G 338.902+0.394	3.4	G 345.198−0.030	2.8	G 351.161+0.697	12
G 336.464−0.157	0.6	G 338.920+0.550	68	G 345.205+0.317	0.6	G 351.242+0.670	0.2
G 336.496−0.271	20	G 338.925+0.557	conf	G 345.407−0.952	1.5	G 351.251+0.652	0.4
G 336.526−0.156	0.3	G 338.925+0.634	conf	G 345.424−0.951	2.5	G 351.382−0.181	10
G 336.703−0.099	0.8	G 338.926+0.634	conf	G 345.441+0.205	4.4	G 351.417+0.645	2932
G 336.809+0.119	11	G 338.935−0.062	14	G 345.487+0.314	2.6	G 351.417+0.646	conf
G 336.822+0.028	21	G 339.053−0.315	117	G 345.505+0.348	733	G 351.445+0.660	conf
G 336.825+0.139	4.5	G 339.064+0.152	8.2	G 345.498+1.467	0.7	G 351.581−0.353	50
G 336.830−0.375	38	G 339.204−0.018	4.2	G 345.576−0.225	0.2	G 351.611+0.172	12
G 336.864+0.005	44.1	G 339.282+0.136	7.1	G 345.807−0.044	0.9	G 351.688+0.171	56

Table A1 *– continued*

Source name	$I_{6.7}$	Source name	$I_{6.7}$	Source name	$I_{6.7}$	Source name	$I_{6.7}$
G 351.775−0.536	206	G 0.167−0.446	0.6	G 8.669−0.356	6.5	G 15.034−0.677	17
G 352.083+0.167	4.1	G 0.212−0.001	4.8	G 8.683−0.368	101	G 15.094+0.192	8.0
G 352.111+0.176	11	G 0.315−0.201	71	G 8.832−0.028	358	G 15.607−0.255	0.2
G 352.133−0.944	30	G 0.316−0.201	0.4	G 8.872−0.493	30	G 15.665−0.499	20
G 352.517−0.155	11	G 0.376+0.040	0.2	G 9.215−0.202	14	G 16.112−0.303	1.0
G 352.525−0.158	0.4	G 0.409−0.504	1.9	G 9.621+0.196	2211	G 16.302−0.196	12
G 352.584−0.185	5.3	G 0.475−0.010	4.8	G 9.619+0.193	36	G 16.403−0.181	0.2
G 352.604−0.225	2.9	G 0.496+0.188	51	G 9.986−0.028	85	G 16.585−0.051	50
G 352.624−1.077	15	G 0.546−0.852	201	G 10.205−0.345	1.1	G 16.662−0.331	1.5
G 352.630−1.067	101	G 0.645−0.042	conf	G 10.287−0.125	11	G 16.831+0.079	7.4
G 352.855−0.201	1.4	G 0.647−0.055	conf	G 10.299−0.146	0.7	G 16.855+0.641	0.9
G 353.216−0.249	0.5	G 0.651−0.049	conf	G 10.320−0.259	13	G 16.864−2.159	20
G 353.273+0.641	7.8	G 0.657−0.041	conf	G 10.323−0.160	148	G 16.976−0.005	0.8
G 353.363−0.166	0.9	G 0.665−0.036	conf	G 10.342−0.142	22	G 17.021−2.403	7.2
G 353.370−0.091	2.4	G 0.666−0.029	conf	G 10.356−0.148	0.3	G 17.029−0.071	0.9
G 353.378+0.438	1.2	G 0.667−0.034	conf	G 10.444−0.018	conf	G 17.638+0.157	5.9
G 353.410−0.360	106	G 0.672−0.031	conf	G 10.472+0.027	conf	G 17.862+0.074	3.2
G 353.429−0.090	16	G 0.673−0.029	conf	G 10.480+0.033	conf	G 18.073+0.077	9.7
G 353.464+0.562	9.6	G 0.677−0.025	conf	G 10.627−0.384	3.3	G 18.159+0.094	6.4
G 353.537−0.091	2.7	G 0.695−0.038	conf	G 10.629−0.333	11	G 18.262−0.244	40
G 354.206−0.038	0.4	G 0.836+0.184	3.7	G 10.724−0.334	1.9	G 18.341+1.768	49
G 354.308−0.110	5.3	G 1.008−0.237	10	G 10.822−0.103	0.1	G 18.440+0.045	3.1
G 354.496+0.083	6.3	G 1.147−0.124	4.0	G 10.886+0.123	14	G 18.460−0.004	15
G 354.615+0.472	277	G 1.329+0.150	0.6	G 10.958+0.022	9.5	G 18.661+0.034	conf
G 354.701+0.299	1.0	G 1.719−0.088	6.7	G 11.034+0.062	0.2	G 18.667+0.025	conf
G 354.724+0.300	13	G 2.143+0.009	18	G 11.109−0.114	25	G 18.733−0.224	4.2
G 355.184−0.419	conf	G 2.521−0.220	0.8	G 11.497−1.485	153	G 18.735−0.227	2.3
G 355.343+0.148	0.9	G 2.536+0.198	53	G 11.903−0.102	7.3	G 18.834−0.300	3.9
G 355.344+0.147	6.1	G 2.591−0.029	2.1	G 11.904−0.141	65	G 18.874+0.053	6.8
G 355.346+0.149	5.6	G 2.615+0.134	1.9	G 11.936−0.150	3.2	G 18.888−0.475	7.1
G 355.538−0.105	2.4	G 2.703+0.040	16	G 11.936−0.616	63	G 18.999−0.239	0.2
G 355.545−0.103	1.0	G 3.253+0.018	5.3	G 11.992−0.272	1.5	G 19.009−0.029	29
G 355.642+0.398	0.8	G 3.312−0.399	0.8	G 12.025−0.031	114	G 19.249+0.267	4.0
G 355.666+0.374	2.1	G 3.442−0.348	0.3	G 12.112−0.126	3.1	G 19.267+0.349	3.3
G 356.054−0.095	0.2	G 3.502−0.200	0.9	G 12.181−0.123	1.7	G 19.365−0.030	22
G 356.662−0.263	11	G 3.910+0.001	4.1	G 12.199−0.033	17	G 19.472+0.170n	conf
G 357.558−0.321	1.5	G 4.393+0.079	11	G 12.202−0.120	0.3	G 19.472+0.170	conf
G 357.559−0.321	1.9	G 4.434+0.129	2.2	G 12.203−0.107	conf	G 19.486+0.151	conf
G 357.922−0.337	0.8	G 4.569−0.079	0.1	G 12.209−0.102	conf	G 19.496+0.115	3.3
G 357.924−0.337	1.7	G 4.586+0.028	1.4	G 12.265−0.051	5.3	G 19.609−0.234	0.5
G 357.965−0.164	3.7	G 4.676+0.276	3.4	G 12.526+0.016	3.7	G 19.612−0.120	0.5
G 357.967−0.163	104	G 4.866−0.171	0.1	G 12.625−0.017	26	G 19.612−0.134	13
G 358.263−2.061	17	G 5.618−0.082	4.7	G 12.681−0.182	836	G 19.614+0.011	5.7
G 358.371−0.468	31	G 5.630−0.294	3.0	G 12.776+0.128	0.3	G 19.667+0.114	2.9
G 358.386−0.483	1.9	G 5.657+0.416	2.8	G 12.889+0.489	100	G 19.701−0.267	13
G 358.460−0.391	0.5	G 5.677−0.027	0.4	G 12.904−0.031	28	G 19.755−0.128	1.9
G 358.460−0.393	9.7	G 5.885−0.393	1.0	G 12.909−0.260	303	G 19.884−0.534	3.0
G 358.721−0.126	4.2	G 5.900−0.430	6.1	G 13.179+0.061	0.5	G 20.081-0.135	0.7
G 358.809−0.085	6.6	G 6.189−0.358	193	G 13.657−0.599	40	G 20.237+0.065	conf
G 358.841−0.737	6.7	G 6.368−0.052	2.7	G 13.696−0.156	2.8	G 20.239+0.065	conf
G 358.906+0.106	1.7	G 6.539−0.108	0.7	G 13.713−0.083	9.0	G 20.364-0.013	5.3
G 358.931−0.030	9.0	G 6.588−0.192	9.6	G 14.101+0.087	141	G 20.733-0.059	1.4
G 358.980+0.084	conf	G 6.610−0.082	15	G 14.230−0.509	1.3	G 20.926-0.050	6.8
G 359.138+0.031	14	G 6.795−0.257	268	G 14.390−0.020	2.5	G 20.963-0.075	1.0
G 359.436−0.104	18	G 6.881+0.093	1.6	G 14.457−0.143	0.7	G 21.023-0.063	1.1
G 359.436−0.102	50	G 7.166+0.131	4.1	G 14.490+0.014	0.5	G 21.407-0.254	14.2
G 359.615−0.243	56	G 7.601−0.139	8.4	G 14.521+0.155	2.4	G 21.562-0.033	18.3
G 359.938+0.170	0.7	G 7.632−0.109	8.7	G 14.604+0.017	2.9	G 21.848-0.240	0.6
G 359.970−0.457	0.7	G 8.139+0.226	7.6	G 14.631−0.577	0.5	G 21.880+0.014	3.7
G 0.092−0.663	34	G 8.317−0.096	5.6	G 14.991−0.121	3.5	G 22.039+0.222	14.4

Table A1 *– continued*

Source name	$I_{6.7}$	Source name	$I_{6.7}$	Source name	$I_{6.7}$	Source name	$I_{6.7}$
G 22.335−0.155	28.7	G 28.146−0.005	26.3	G 32.825−0.328	0.8	G 41.075−0.125	0.2
G 22.356+0.066	14.0	G 28.201−0.049	4.8	G 32.914−0.096	0.1	G 41.121−0.107	0.3
G 22.435−0.169	28.7	G 28.282−0.359	2.5	G 32.963−0.340	0.3	G 41.123−0.220	1.3
G 23.003+0.124	2.9	G 28.305−0.387	54.7	G 32.992+0.034	12.5	G 41.156−0.201	1.0
G 23.010−0.410	643	G 28.321−0.011	2.4	G 33.093−0.073	26.1	G 41.226−0.197	9.0
G 23.126+0.395	1.0	G 28.397+0.081	11.4	G 33.133−0.092	13.8	G 41.348−0.136	25.2
G 23.207−0.377	79.4	G 28.523+0.127	0.5	G 33.317−0.360	1.4	G 42.034+0.190	27.2
G 23.257−0.241	9.6	G 28.532+0.129	1.7	G 33.393+0.010	35.4	G 42.13+0.52	0.2
G 23.365−0.291	0.6	G 28.608+0.018	1.5	G 33.486+0.040	3.7	G 42.304−0.299	4.0
G 23.389+0.185	66.9	G 28.687−0.283	1.2	G 33.641−0.228	128.4	G 42.435−0.260	2.0
G 23.437−0.184	99.6	G 28.700+0.406	0.4	G 33.634−0.021	0.7	G 42.698−0.147	4.9
G 23.440−0.182	62.8	G 28.817+0.365	11.8	G 33.725−0.120	3.3	G 43.038−0.453	8.9
G 23.484+0.097	10.8	G 28.832−0.253	115.6	G 33.852+0.018	3.0	G 43.074−0.077	3.3
G 23.657−0.127	37.8	G 28.842+0.493	3.1	G 33.980−0.019	4.6	G 43.149+0.013	9.3
G 23.706−0.198	47.6	G 28.848−0.228	2.1	G 34.096+0.018	5.5	G 43.165+0.013	conf
G 23.885+0.060	1.4	G 28.861+0.065	0.3	G 34.244+0.133	conf	G 43.167−0.004	1.0
G 23.901+0.077	0.5	G 29.320−0.162	3.7	G 34.257+0.153	conf	G 43.171+0.005	28.0
G 23.966−0.109	conf	G 29.603−0.625	1.7	G 34.267−0.210	5.7	G 43.175−0.015	0.1
G 23.986−0.089	conf	G 29.863−0.044	107.0	G 34.396+0.222	13.4	G 43.180−0.518	3.2
G 23.996−0.100	conf	G 29.955−0.016	214.7	G 34.751−0.093	5.3	G 43.795−0.127	35.2
G 24.148−0.009	27.9	G 29.978−0.047	87.5	G 34.757+0.025	0.8	G 43.890−0.784	17.6
G 24.329+0.144	14.0	G 29.993−0.282	0.9	G 34.791−1.387	35.5	G 44.310+0.041	0.5
G 24.461+0.198	9.0	G 30.010−0.273	0.6	G 34.82+0.35	0.1	G 44.644−0.516	0.1
G 24.493−0.039	17.4	G 30.198−0.169	30.4	G 35.025+0.350	28.2	G 45.071+0.132	2.8
G 24.541+0.312	21.1	G 30.225−0.180	25.6	G 35.132−0.744	44.1	G 45.380−0.594	1.5
G 24.634−0.324	4.5	G 30.317+0.070	14.7	G 35.197−0.743	conf	G 45.445+0.069	0.9
G 24.676−0.150	4.4	G 30.370+0.482	1.3	G 35.197−0.743n	conf	G 45.467+0.053	2.2
G 24.790+0.083a	conf	G 30.400−0.296	7.0	G 35.200−1.736	601.3	G 45.473+0.134	4.8
G 24.790+0.083b	conf	G 30.419−0.232	7.1	G 35.247−0.237	0.5	G 45.493+0.126	4.3
G 24.790+0.084	0.6	G 30.423+0.466	1.9	G 35.397+0.025	0.3	G 45.804−0.356	8.4
G 24.791+0.082	0.8	G 30.542+0.011	0.4	G 35.588+0.060	0.4	G 46.066+0.220	0.6
G 24.850+0.087	conf	G 30.58−0.14	0.1	G 35.793−0.175	20.4	G 46.115+0.387	1.2
G 24.920+0.088	3.1	G 30.589−0.043	7.9	G 36.115+0.552	57.6	G 48.902−0.273	0.3
G 24.943+0.074	1.7	G 30.703−0.068	66.9	G 36.634−0.203	0.3	G 48.990−0.299	0.3
G 25.226+0.288	0.5	G 30.760−0.052	64.4	G 36.705+0.096	5.8	G 49.043−1.079	52.4
G 25.270−0.434	2.9	G 30.771−0.804	10.5	G 36.839−0.022	7.6	G 49.265+0.311	14.1
G 25.382−0.182	2.9	G 30.780+0.230	20.7	G 36.918+0.483	0.4	G 49.349+0.413	8.2
G 25.407−0.170	2.6	G 30.788+0.204	48.9	G 37.030−0.038	4.8	G 49.416+0.326	15.3
G 25.411+0.105	10.7	G 30.774+0.078	0.4	G 37.043−0.035	15.3	G 49.417+0.324	3.4
G 25.494+0.062	2.0	G 30.818−0.057	21.4	G 37.430+1.518	233.9	G 49.470−0.371	conf
G 25.613+0.226	0.3	G 30.818+0.273	2.2	G 37.479−0.105	26.4	G 49.471−0.369	conf
G 25.650+1.049	48.7	G 30.822−0.053	8.4	G 37.546−0.112	4.6	G 49.482−0.402	conf
G 25.710+0.044	550.5	G 30.851+0.123	0.9	G 37.554+0.201	8.4	G 49.489−0.369	conf
G 25.826−0.178	90.1	G 30.898+0.161	134.5	G 37.598+0.425	18.0	G 49.490−0.388	conf
G 25.838−0.378	0.5	G 30.960+0.086	0.3	G 37.735−0.112	0.2	G 49.599−0.249	66.9
G 25.920−0.141	0.8	G 30.972−0.142	23.8	G 37.753−0.189	1.6	G 49.617−0.360	0.2
G 26.422+1.685	2.6	G 30.973+0.562	0.3	G 37.767−0.214	0.1	G 50.035+0.582	6.3
G 26.545+0.423	0.3	G 30.980+0.216	1.3	G 38.037−0.300	13.8	G 50.315+0.676	4.3
G 26.527−0.267	3.5	G 31.047+0.356	8.9	G 38.119−0.229	7.0	G 50.779+0.152	2.9
G 26.598−0.024	11.8	G 31.059+0.093	11.5	G 38.203−0.067	19.0	G 51.679+0.719	0.9
G 26.601−0.221	17.4	G 31.076+0.457	0.8	G 38.255−0.200	0.7	G 51.818+1.250	1.1
G 26.648+0.018	1.2	G 31.122+0.063	1.0	G 38.258−0.074	5.8	G 52.199+0.723	3.9
G 27.011−0.039	1.2	G 31.158+0.046	1.3	G 38.565+0.538	1.0	G 52.663−1.092	5.6
G 27.221+0.136	26.1	G 31.182−0.148	3.7	G 38.598−0.212	0.2	G 52.922+0.414	4.5
G 27.220+0.261	5.9	G 31.281+0.061	158.6	G 38.653+0.088	0.4	G 53.036+0.113	0.6
G 27.286+0.151	21.8	G 31.412+0.307	47.8	G 38.916−0.353	1.9	G 53.142+0.071	0.6
G 27.365−0.166	65.7	G 31.581+0.077	7.4	G 39.100+0.491	28.1	G 53.618+0.035	3.6
G 27.500+0.107	1.0	G 31.594−0.192	0.9	G 39.388−0.141	0.7	G 56.963−0.235	0.2
G 27.757+0.050	0.5	G 32.045+0.059	139.1	G 40.282−0.219	63.7	G 57.610+0.025	11.8
G 27.783−0.259	3.2	G 32.082+0.078	7.9	G 40.425+0.700	31.2	G 58.775+0.644	7.4
G 27.784+0.057	3.3	G 32.516+0.323	0.5	G 40.597−0.719	0.3	G 59.634−0.192	2.2
G 27.869−0.235	0.1	G 32.744−0.075	103.7	G 40.622−0.138	5.5	G 59.783+0.065	27.0
G 28.011−0.426	8.3	G 32.802+0.193	1.1	G 40.934−0.041	1.5	G 59.833+0.672	17.7

This paper has been typeset from a TEX/LATEX file prepared by the author.